SYNTHESIS OF WATER-SOLUBLE BIMETALLIC NANOCLUSTERS WITH MULTIFUNCTIONALITIES

DOU XINYUE

NATIONAL UNIVERSITY OF SINGAPORE

2014

SYNTHESIS OF WATER-SOLUBLE BIMETALLIC NANOCLUSTERS WITH MULTIFUNCTIONALITIES

DOU XINYUE

(*B.Eng. Shandong University of Technology, China*)

A THESIS SUBMITTED FOR THE DEGREE OF MASTER OF ENGINEERING

DEPARTMENT OF CHEMICAL AND BIOMOLECULAR ENGINEERING

NATIONAL UNIVERSITY OF SINGAPORE

2014

DECLARATION

I hereby declare that the thesis is my original work and it has been written by me in its entirety. I have duly acknowledged all the sources of information which have been used in the thesis.

This thesis has also not been submitted for any degree in any university previously.

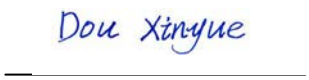

Dou Xinyue

03 January 2014

ACKNOWLEDGEMENTS

First and foremost, I would like to convey my greatest appreciation to my supervisor, Prof. Xie Jianping, for his encouragement, invaluable guidance, patience and understanding throughout my entire master study. Prof. Xie's profound knowledge, research enthusiasm and vigorous methodology guided me to finish my master projects successfully. I am also thankful to him for his strong support in other aspects of life than research.

I wish to express my sincere thanks to all my friends and colleagues in the research group, Dr. Yu Yong, Mr. Luo Zhentao, Mr. Yao Qiaofeng, Dr. Yu Yue, Ms. Lu Meihua, Ms. Liu Qing, Mr. Li Jingguo, Ms. Zheng Kaiyuan and Mr. Yuan Xun. In addition, I am also thankful to Mr. Toh Keng Chee, Mdm. Teo Ai Peng, Mr. Qin Zhen, Mr. Lim You Kang, Dr. Yang Liming, and other technical staff in the department for their assistance and support.

The financial support from National University of Singapore is also acknowledged.

TABLE OF CONTENTS

SUMMARY

Ultrasmall bimetallic nanoclusters (or bi-MNCs for short) have recently emerged as a new class of multi-functional nanoparticles (NPs) due to their ultrasmall size (typically below 2 nm), unique molecular-like properties (e.g., quantized charging and strong luminescence), controlled cluster compositions (at the atomic level), and synergistic physicochemical properties (integration of two metal species into one cluster). However, previous studies all focused on the one-step synthesis of hydrophobic thiolate-protected bi-MNCs, and there is no successful attempt in synthesizing water-soluble and atomically precise bi-MNCs, let alone engineering the surface functionalities of bi-MNC's ligand shell. Moreover, synthesis of water-soluble and highly luminescent bi-MNCs is still a challenge, and the corresponding luminescence mechanism is also unclear. All such issues may constrict the advances of bi-MNCs in bioapplications where biocompatibility (e.g., water solubility), multi-functional ligand surface, and/or high luminescence are required. In this thesis, two novel synthetic strategies have been developed to synthesize water-soluble and atomically precise AuAg bi-MNCs with either tunable metallic compositions/surface functionalities or high luminescence.

Firstly, a series of water-soluble $(AuAg)_{25}$ bi-MNCs protected by mono- and bi-thiolate ligands have been synthesized via NaOH-mediated $NaBH_4$ reduction method. Compositions of both the metallic core and ligand shell can be continuously tuned by varying the feeding ratios of metal precursors and hetero-ligands, greatly expanding the combinational functionalities of the NCs.

Secondly, A simple strategy has been developed to synthesize highly luminescent thiolated Au@Ag bi-MNCs by using Ag(I) ions to bridge small Au(I)-thiolate motifs on the weakly luminescent thiolated Au NCs, leading to the formation of large Au(I)/Ag(I)-thiolate motifs on the NC surface and thus generating strong luminescence via aggregation-induced emission. The method and products developed here are of interest not only because they can provide multifunctional candidates for bioapplications, but also they can shed some light on the design of new synthetic strategies for more bimetallic NCs and the multi-functionalization of nanoscale materials.

LIST OF FIGURES

LIST OF SYMBOLS

AIE	aggregation induced emission
Bi-MNCs	bimetallic nanoclusters
Cys	cysteine
Cystm	cysteamine
DHB	2,5-dihydroxybenzoic acid
ESI	electrospray ionization
EXAFS	extended X-ray absorption fine structure
GSH	L-glutathione reduced
ICP-MS	inductively coupled plasma-mass spectrometry
MALDI-TOF	matrix assisted laser desorption ionization-time of flight
MetH	2-mercaptoethanol
MHA	6-mercaptohexanoic acid
MOA	8-mercaptooctanoic acid
MSA	mercaptosuccinic acid
MUA	11-mercaptoundecanoic acid
MNCs	metal nanoclusters
MNPs	metal nanoparticles
MWCO	molecular weight cut off
PAGE	polyacrylamide gel electrophoresis
PEG	Poly(ethylene glycol)
PL	photoluminescence
QY	quantum yield
TCSPC	time-correlated single-photon counting
TEM	transmission electron microscopy
THPC	tetrakis(hydroxymethyl)phosphonium chloride

QY	quantum yield
τ	lifetime
XPS	x-ray photoelectron spectroscopy

CHAPTER 1 INTRODUCTION

1.1 Background

Noble metal nanoclusters (MNCs) such as Au and Ag NCs, typically comprising of a hundred metal atoms or less, are a subclass of metal nanoparticles (MNPs).[1, 2] MNCs contain a small metal core with sizes below 2 nm and an organic ligand shell.[3-5] Particles in this sub-2 nm size range show characteristic strong quantum confinement effects, which result in their discrete and size-dependent electronic transitions, as well as unique geometric cluster structures, distinctively different from their larger counterparts – MNPs with core sizes above 2 nm, which feature with quasi-continuous electronic states and adopt a face centered cubic (*fcc)* atomic packing.[2, 6] Consequently, sub-2 nm sized MNCs display unique molecular-like properties, such as magnetism,[7, 8] HOMO-LUMO transitions,[9-11] quantized charging,[10, 12] and strong luminescence.[13-16] Such intriguing physicochemical properties have made MNCs good platforms to address some key challenges in the fields of catalysis, energy conversion, drug delivery, sensor development, biomedicine, and nanophotonics.[17-26] The diverse yet promising applications of MNCs have also motivated a rapid progress in the development of functional MNCs.[27-29]

In the wake of extensive development of mono-metallic NCs (mono-MNCs for short), more recently, the cluster community has begun to investigate functional NCs comprising of two or more metal species, and such bi- or multi-metallic NCs (bi- or multi-MNCs for short) have quickly emerged as a new and promising member in the MNC family.[30-35] In principle, integrating two or more metal species into one cluster (e.g., bi-MNCs) may

have the following attractive features as compared to their mono-MNC analogues: 1) the physicochemical properties of two metal species can be easily integrated into one bi-MNC;[33, 36] 2) some synergistic effects such as strong luminescence could be realized in bi-MNCs;[34] and 3) the electronic structures of bi-MNCs could be further tailored via controlling their sizes, compositions,[37, 38] and structures (e.g., core-shell, alloy, and hetero-structure),[36, 39] typically at the atomic level. In view of the obvious advantages of bi-MNCs, a number of synthetic strategies have been developed for bi-MNCs, with a special focus on those bi-MNCs featuring with good monodispersity and/or strong luminescence,[30-35, 40] and applications of such bi-MNCs in a wide range of fields such as catalysis, sensors, and human health, have recently surfaced to the community.[41-44] Therefore, there is a pressing need to survey recent advances of the synthesis and applications of bi-MNCs, which could shed some light on the design of novel synthetic strategies for high-quality bi-MNCs, further paving their way towards practical applications.

This Chapter will be organized in four sections. We will firstly summarize previously developed general synthetic methods for monodisperse and/or luminescent bi-MNCs, with a special focus on the understanding of underlying principles in those synthetic strategies. We will only cover the synthesis of bi-MNCs although some synthetic strategies of bi-MNCs are also quite similar to that of mono-MNCs. The synthetic strategies for mono-MNCs have been well discussed in several excellent review articles.[1-6, 16, 27, 29, 45-47] In the second section, we will discuss recent advances in the applications of bi-MNCs, including catalysis, sensor development, and biomedicine. The research gaps

and objectives, and outline of this thesis will be listed in the third and fourth sections, respectively.

1.2 Synthesis of Monodisperse and/or Luminescent Bi-MNCs

Ligand-protected bi-MNCs can be roughly categorized into three types according to their protecting ligands. They are thiolate-,[31] protein-,[48] and DNA-protected[49] bi-MNCs, similar to the classification of their mono-MNC analogues.[3] Among these bi-MNCs, those protected by thiolate ligands have been studied more intensively because of their good stability in solution (via the strong thiolate-metal interaction), unique metallic-core@ligand-shell structure, low and controllable molecular weight, rich surface chemistry, low cost, and facile synthesis. In this section, we will focus our discussion on the synthetic strategies for thiolate-protected bi-MNCs.

A number of classifications regarding to the synthetic strategies are present in the literature according to different criteria, such as different ligands, precursors, reduction kinetics, reaction environments, and synthetic procedures. Here we simply classify the synthetic strategies for bi-MNCs into two types according to the preparation steps, which are one- and two-step synthesis. One-step synthesis (Figure 1.1a), generally described as co-reduction method, can synthesize bi-MNCs in a one-pot manner via a simultaneous reduction of two metal ions in the reaction solution, in the presence of a particular protecting ligand. This method is straightforward and is directly derived from the synthesis of mono-MNCs.[30] Therefore, the one-step method is one most common strategy to prepare bi-MNCs. In contrast, the two-step method involves two steps (Figure 1.1b), which are i) preparation of

the precursors/intermediates, such as mono-MNCs, bi-MNPs, and bi-MNCs; and ii) post-treatment of the precursors/intermediates to synthesize bi-MNCs by incorporating a second metal in mono-MNCs or etching bi-MNCs/MNPs intermediates. In particular, there are three efficient approaches for the post-treatment of the precursors/intermediates to form bi-MNCs. They are galvanic replacement,[41] anti-galvanic replacement,[50, 34] and thiol-etching.[51] These approaches are summarized in the following section.

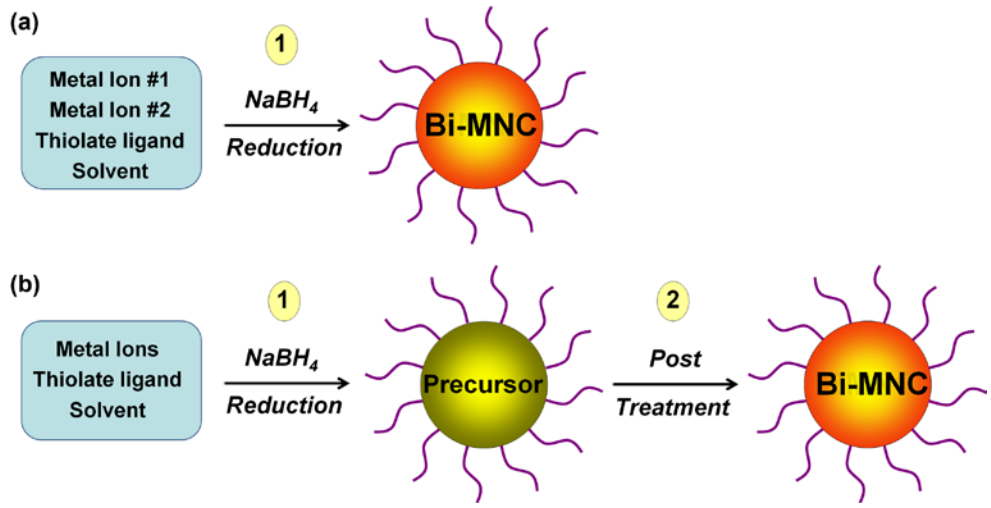

Figure 1.1 Schematic illustration of (a) one-step and (b) two-step synthesis of bi-MNCs.

1.2.1 One-Step or Co-Reduction Synthesis of Bi-MNCs

When discussing the historical evolution of one-step synthesis of bi-MNCs, it is inevitable to mention the one-step synthesis method of mono-MNCs as the same synthetic strategy in the mono-MNC system was perfectly shifted to the synthesis of bi-MNCs. In 1994, Brust et al. reported a one-step synthesis of thiolate-protected Au NPs by using a strong reducing agent, sodium borohydride $NaBH_4$, to reduce Au ions in the presence of thiolate ligands.[52] Recently, smaller thiolate-protected Au NCs with discrete sizes, such as Au_{15}, Au_{18},[53, 54] Au_{19},[55] Au_{20},[56] Au_{24},[57] Au_{25},[11, 58-60] Au_{28},[61] Au_{29},[62]

Au_{36},[63] Au_{38},[64] Au_{40},[65] Au_{67},[66] Au_{102},[67] Au_{103-5},[68] Au_{144},[69] and Au_{187} NCs,[70] have been successfully synthesized by using Brust or Brust-like method. Among these atomically precise Au NCs, the cluster structures of thiolated Au_{25},[11, 57] Au_{28},[61] Au_{36},[63] Au_{38},[64] and Au_{102}[67] NCs have been successfully resolved by using single crystal X-ray diffraction. Closely following the rapid advances in mono-MNCs, a number of monodisperse bi-MNCs have been successfully synthesized by using Brust or Brust-like method.[30-33, 42, 47, 71-83]

In general, two metal ions such as Au^{3+} and Ag^{+}, are simultaneously reduced by the addition of a certain amount of $NaBH_4$, leading to the formation of bi-MNCs in the reaction solution. Similar to the mono-MNCs, where thiolated Au_{25}, Au_{38}, and Au_{144} NCs are the most common and well-studied NC species because of their superior stability in solution, intriguing optical properties, resolved cluster structures, and facile syntheses, bi-MNCs comprising of 25, 38, and 144 metal atoms are three most common species that have been synthesized by using the one-step or co-reduction method.[30-33, 72-74, 76, 78-85] A number of efficient protocols have been developed. However, the formation of bi-MNCs in the co-reduction or one-step method could be influenced by several parameters, such as the atomic radius and redox potential of the metal pairs, the possible interactions between the metal pairs, and the affinity of ligands with the metal pairs. Such parameters also determine the structure symmetry and the superatom electron saturability of bi-MNCs, which further dictate the incorporation of the second metal in the mono-MNCs, such as the ratio of the doping metals in bi-MNCs. Ag, Cu, Pd, and Pt are most common metals that can be incorporated in Au NCs for the formation of bi-MNCs. However, the as-synthesized Au-based bi-MNCs by

doping with Ag, Cu, Pd and Pt, are remarkably different in their compositions, electronic structures, and stability in solution. In this section, we will discuss the synthesis of such Au-based bi-MNCs doped with Ag, Cu, Pd, and Pt, with an additional focus on the evolution of their physicochemical properties during the doping.

(a) Au-Ag NCs

Au, with an atomic number of 79, and Ag, with an atomic number 47, are in the same IB group, and they feature with many similar physicochemical properties. For example, Au and Ag atoms have nearly identical atomic radius (1.44 Å),[74, 82] and both have a valence electron in the s shell. Similar to the aurophilic interaction between Au atoms, Au and Ag also feature with a strong metallophilic interaction.[86] The relatively strong interaction between Au and Ag can facilitate the synthesis of Au-Ag NCs, with a minimized distortion in their cluster structure. However, Au and Ag have different redox potentials: $AuCl_4^-/Au^0$: ~1 V and Ag^+/Ag: 0.8 V,[87] resulting in different reduction kinetics of Au^{3+} and Ag^+ in a particular reaction system, which may lead to a phase separation of Au and Ag, forming mono-metallic Au and Ag NCs in the reaction solution.[88] One efficient way to address this issue is to delicately balance the redox potential of Au and Ag. For example, the addition of thiolate ligands can effectively address this challenge as the thiolate ligands have a stronger affinity with Au compared to Ag, which could minimize the difference in their redox potentials, leading to a better control of the synthesis of high-quality Au-Ag NCs upon the reduction.

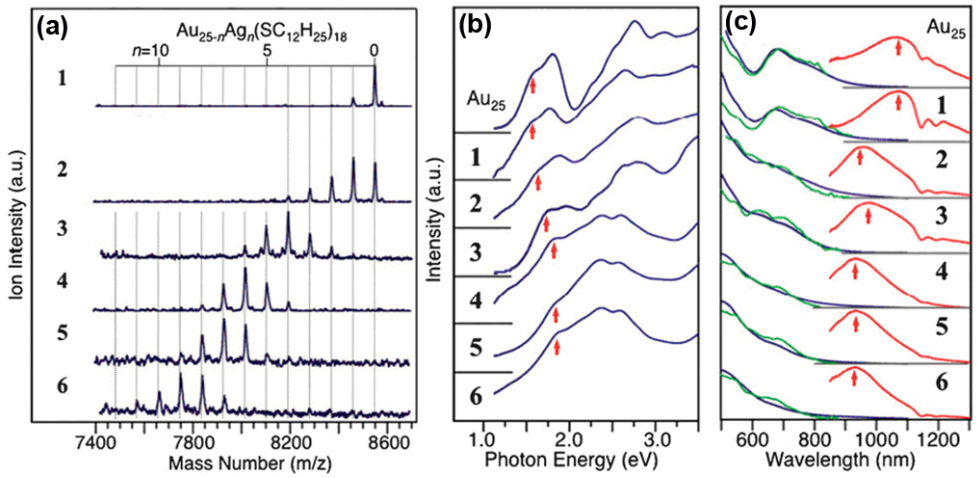

Figure 1.2 (a) MALDI-TOF mass spectra of $Au_{25-n}Ag_n(SC_{12}H_{25})_{18}$ NCs at different feeding ratios of Au^{3+}/Ag^{+}: (1) 22:3; (2) 19:6; (3) 15:10; (4) 10:15; (5) 8:17; (6) 5:20. (b) Optical absorption spectra, and (c) optical absorption (blue), photoemission (red), and photoexcitation (green) spectra of $Au_{25}(SC_{12}H_{25})_{18}$ and $Au_{25-n}Ag_n(SC_{12}H_{25})_{18}$ NCs. Reproduced with permission.[31] Copyright 2010, Royal Society of Chemistry.

Recently, Negishi et al. applied the two-phase Brust method at a low temperature of 0 ^{o}C to synthesize Au-Ag NCs, and have successfully obtained a series of $Au_{25-n}Ag_n(SC_{12}H_{25})_{18}$ NCs with different compositions (n is from 0 to 11, Figure 1.2a) by adjusting the feeding ratios of $HAuCl_4$ to $AgNO_3$.[31] Interestingly, the electronic structures of $(AuAg)_{25}$ NCs can be rationally tuned by doping different number of Ag atoms in the Au-Ag NCs, which were also reflected in their respective UV-vis absorption (Figure 1.2b) and luminescence spectra (Figure 1.2c). It is well-documented that thiolated Au_{25} NCs consist of an icosahedral Au_{13} core and six -S-[Au-S-]$_2$ oligomer motifs (Figure 1.3a).[11, 58, 82] The optical absorption of such thiolated Au_{25} in the range of 1–2.5 eV was attributed to the transitions from the high-lying Au 6sp orbital to the unoccupied low-lying Au 6sp orbital of the central Au_{13} core. According to the continuous shift of the electronic structures of $Au_{25-n}Ag_n(SC_{12}H_{25})_{18}$ NCs, Negishi et al. hypothesized that the Ag atoms were progressively incorporated in the central Au_{13} core with the increase of Ag doping. This

hypothesis was also in good agreement with the experimental observations that the binding energy of the Ag 3d of the Au-Ag NCs (367.6 eV) was lower than that of the metallic Ag^0 (367.9 eV). Such binding energy difference was most likely due to the strong Au-Ag interaction. This data matched nicely with the theoretical studies, which also explained why the maximum doping of Ag atoms in $(AuAg)_{25}$ NCs was 13. Recently, other thiolate ligands such as hydrophobic HSC_2H_4Ph have also been used to prepare $Au_{25-n}Ag_n(SR)_{18}$ NCs.[32, 82, 89] Similar observations have been obtained, which suggest that the formation of $(AuAg)_{25}$ NCs was not solely dependent on the type of thiolate ligands.

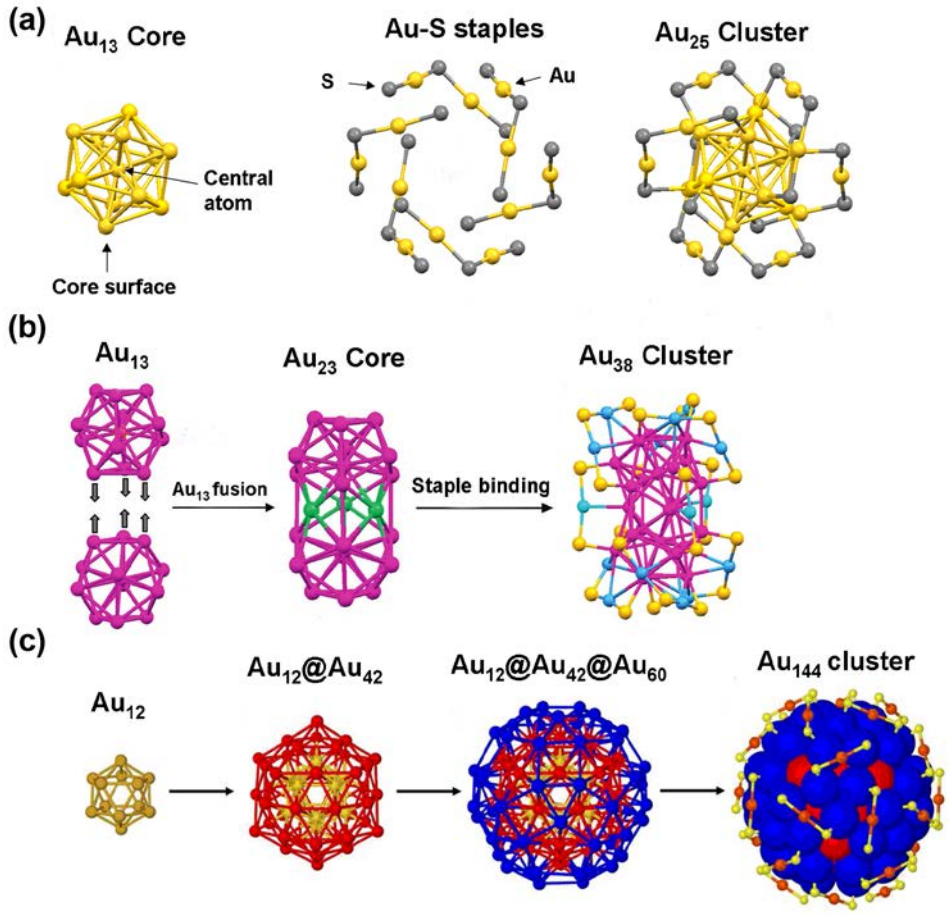

Figure 1.3 Cluster structures of thiolated (a) Au_{25}, (b) Au_{38}, and (c) Au_{144} NCs. Reproduced with permission.[64, 82, 90] Copyright 2009, 2010, and 2013, American Chemical Society.

Besides thiolated $(AuAg)_{25}$ NCs, $(AuAg)_{144}(SC_2H_4Ph)_{60}$ and $(AuAg)_{38}(SC_2H_4Ph)_{24}$ NCs have also been successfully synthesized and investigated by Dass et al.[33, 79] Up to 60 and 12 Ag atoms can be incorporated in the $(AuAg)_{144}$ and $(AuAg)_{38}$ NCs, respectively. As shown in Figure 1.3b and 1.3c, the theoretical studies suggest that the Au_{144} NC adopts a 3-shell structure including a concentric 12-atom (hollow), and one 42-atom and 60-atom shell, which are protected by 30 -S-[Au-S-]$_1$ oligomers.[90] Furthermore, the cluster structure of Au_{38} NCs has been determined by single crystal X-ray diffraction, showing a Au_{23} core capped with 6 long -S-[Au-S-]$_2$ and 3 short -S-[Au-S-]$_1$ oligomers.[64] Similar to $(AuAg)_{25}$ NCs, the 12 Ag atoms of the $(AuAg)_{38}$ NCs were suggested to be in the M_{23} core, while the 60 Ag atoms of the $(AuAg)_{144}$ NCs were selectively incorporated in the third shell of M_{60}, especially if the geometric symmetry of the structure was also considered.[91]

More recently, the cluster structure of one Au-Ag NC species was successfully resolved by Zheng et al. In this study, a new species of thiolated $Au_{12}Ag_{32}$ NC has been successfully synthesized by co-reducing Au^{3+}-Ag^{+} ions in a mixed solvent of dichloromethane/methanol.[40] As shown in Figure 1.4, the $Au_{12}Ag_{32}$ NC adopts a two-shell "concentric icosahedral Au_{12}@dodecaheral Ag_{20}" core protected by 6 $Ag_2(SR)_5$ oligomers, in which Ag atoms bind to three thiolate ligands in a planar $Ag(SR)_3$ configuration. The as-synthesized $Au_{12}Ag_{32}$ NCs carried four negative charges and thus fulfilled the superatom criteria of 18-shell electrons, which explained their superior thermal stability. This study is of great interest not only because it is the first successful attempt in synthesizing thiolated Au-Ag NCs with fixed number of

Au and Ag atoms, but also because it resolves the cluster structure of Au-Ag NCs which could shed light on the structural evolution of bi-MNCs.

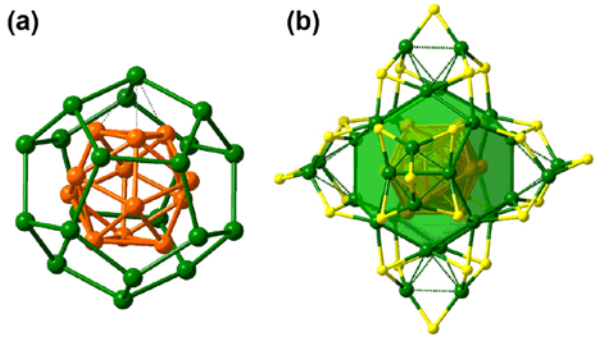

Figure 1.4 Cluster structure of $Au_{12}Ag_{32}(SR)_{30}$ NCs. (a) Two-shell $Au_{12}@Ag_{20}$ core of the $Au_{12}Ag_{32}(SR)_{30}$ NCs. (b) Arrangement of six $Ag_2(SR)_5$ motif units on the surface of $Au_{12}Ag_{32}(SR)_{30}$ NCs. Reproduced with permission.[40] Copyright 2013, Nature Publishing Group.

To date, thiolated Au-Ag NCs are the most studied NC species in the one-step synthesis method. A variety of thiolate ligands have been utilized for the synthesis of Au-Ag NCs. However, the as-synthesized products are often a mixture of Au-Ag NCs with a certain distribution of Au and Ag atoms although the total number of metal atoms could be a constant. This result could be due to the indistinguishable atomic radius (1.44 Å) between Au and Ag. The synthesis of Au-Ag NCs with a precise control of the Au and Ag number is still challenging. In addition, besides $(AuAg)_{25}$, $(AuAg)_{38}$, and $(AuAg)_{144}$ NCs, more bi-MNC species with discrete core sizes, such as M_{15}, M_{18}, M_{22}, and M_{102}, are expected to be synthesized in the future to enrich the library of bi-MNCs. In addition, more experimental evidences on the electronic structures of bi-MNCs are required, which could serve the basis for deeper understandings of the physicochemical properties of bi-MNCs and provide a guideline for further functionalization of bi-MNCs.

(b) Au-Cu NCs

Cu, with an atomic number of 29, lies in the same group as Au in the periodic table. Cu (1.28 Å) has a smaller atomic radius than Au (1.44 Å),[74] and the interaction of Cu-Au is even stronger than that of Au-Au.[92] Therefore the incorporation of Cu in Au NCs may cause a remarkable distortion in their geometric structure, which could decrease the stability of Au-Cu NCs. In addition, the redox potential of Au ($AuCl_4^-/Au^0$: ~1 V) is much higher than that of Cu (Cu^{2+}/Cu: ~0.34 V),[87] where the Cu^{2+} ions are even more difficult to be reduced than Ag^+ ions (Ag^+/Ag: ~0.8 V). The above considerations indicate that it could be relatively difficult to prepare Au-Cu NCs compared to Au-Ag NCs. Again, this challenge could be partially addressed by the addition of thiolate ligands as the protecting molecules, where the thiolate ligands can decrease the redox potential difference of Au and Cu.

For example, Negishi et al. adapted one efficient synthesis method for mono-MNCs to prepare Au-Cu NCs. They have successfully obtained $Cu_nAu_{25-n}(SC_2H_4Ph)_{18}$ NCs by reducing Au^{3+} and Cu^{2+} ions in methanol and in the presence of PhC_2H_4SH. Thereafter, the as-synthesized $Cu_nAu_{25-n}(SC_2H_4Ph)_{18}$ NCs were extracted by using acetonitrile.[74] By electrospray ionization mass spectrometry (ESI-MS), they observed that the number of Cu atoms in $Cu_nAu_{25-n}(SC_2H_4Ph)_{18}$ varied very slightly with the increase of the feeding ratios of Au^{3+}/Cu^{2+}. In addition, this value (the number of Cu atoms in the Au-Cu NCs) was always below 6 regardless of the feeding ratios of Au^{3+}/Cu^{2+}. This result has been further confirmed by applying another thiolate ligand, $C_8H_{17}SH$, for the synthesis of Au-Cu NCs. Cu has a smaller atomic radius (1.28 Å), and the doping of Cu in Au NCs would significantly distort

the NC structure. Therefore, $(AuCu)_{25}$ NCs consisting of >5 Cu atoms may not survive or preserve in the reaction solution during the synthesis. Consequently, only up to five Cu atoms can be incorporated in the $Au_{25}(SR)_{18}$. In addition, although $Cu_nAu_{25-n}(SC_2H_4Ph)_{18}$ NCs comprising of ≤5 Cu atoms can be obtained, their stability was much lower than that of $Au_{25}(SC_2H_4Ph)_{18}$ NCs, most likely because of the structure distortion due to the Cu insertion. This hypothesis has been further confirmed by a theoretical study.[93] More recently, Jin et al. observed a spontaneous de-alloying process in which the initially formed $Cu_nAu_{25-n}(SC_2H_4Ph)_{18}$ NCs were converted to $Au_{25}(SC_2H_4Ph)_{18}$ NCs after a certain period of incubation, suggesting the relatively poor stability of Au-Cu NCs in solution compared to Au NCs.[32]

The practical applications often require good stability of functional NCs, which has motivated the studies towards the improvement of the stability of Au-Cu NCs. Very recently, Negishi et al. have successfully obtained a series of highly stable $Cu_nAu_{25-n}(SeC_8H_{17})_{18}$ NCs, with up to 9 Cu atoms per cluster, by using selenolate as the protecting ligands.[76] The selenolate ligands showed stronger interaction with metals compared to thiolate ligands, leading to the formation of Au-Cu NCs with an improved stability, which could also allow more Cu atoms to be incorporated in Au NCs. The authors also observed that with the increase of Cu doping, the HOMO-LUMO gaps of the Au-Cu NCs were gradually decreased, and their photoluminescence emissions were gradually shifted to longer wavelengths.

Another recent breakthrough in Au-Cu NC studies is the determination of cluster structures of three Au-Cu NC species. Zheng et al. have successfully

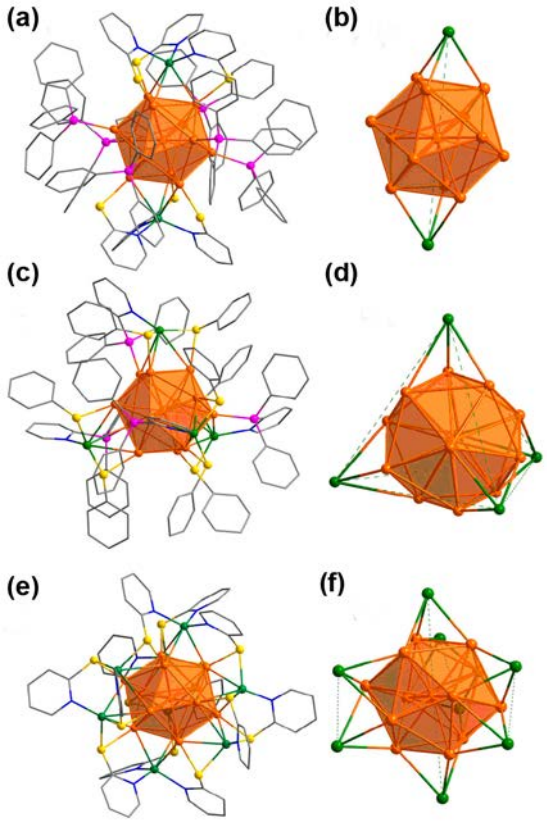

Figure 1.5 Cluster structures of (a) $[Au_{13}Cu_2(PPh_3)_6(SPy)_6]^+$, (c) $[Au_{13}Cu_4(PPh_2Py)_4(SC_6H_4\text{-tert-}C_4H_9)_8]^+$, and (e) $[Au_{13}Cu_8(PPh_2Py)_{12}]^+$ NCs. (b, d, and f) Distributions of corresponding Cu atoms on the Au_{13} core. Color legend: Au/golden sphere; Cu/green sphere; S/yellow sphere; P/pink sphere; C/gray stick; N/blue stick. All H atoms in both clusters and tert-butyl groups in $[Au_{13}Cu_4(PPh_2Py)_4(SC_6H_4\text{-tert-}C_4H_9)_8]^+$ are omitted. Reproduced with permission.[94] Copyright 2013, American Chemical Society.

synthesized and resolved the structures of three Au-Cu NCs $[Au_{13}Cu_2(PPh_3)_6(SPy)_6$, $Au_{13}Cu_4(PPh_2Py)_4(SC_6H_4\text{-tert-}C_4H_9)_8$, and $Au_{13}Cu_8(PPh_2Py)_{12}]$ protected by a mixed-layer of thiolate and phosphine ligands.[94] As shown in Figure 1.5, these Au-Cu NCs have an icosahedral Au_{13} core faced-capped by two (Figure 1.5b), four (Figure 1.5d), or eight Cu atoms (Figure 1.5f), respectively. All the face-capping Cu atoms in the Au-Cu NCs are triply coordinated by thiolate or pyridyl groups. Interestingly, the surface ligands can control the exposure of Au sites in the Au-Cu NCs. For example, while the surface ligands on $Au_{13}Cu_2$ and $Au_{13}Cu_4$ completely block the Au sites, the presence of twelve 2-pyridylthiolate ligands in $Au_{13}Cu_8$ NCs

provides open space for the Au sites. All three Au-Cu NCs carry 1+ charge, and they are 8-shell electron superatoms showing optical bandgaps of 1.8–1.9 eV.

To date, although the cluster structures of mixed-ligand-protected $Au_{13}Cu_n$ NCs (n = 2, 4, 8) have been clearly resolved, more efforts are still required to resolve the cluster structures of purely thiolate-protected Au-Cu NCs, which could also provide good platforms to study the ligand-structure correlation. In addition, all thiolate-protected Au-Cu NCs have been synthesized so far are within the M_{25} domain, and more efforts are needed to develop efficient methods to synthesize thiolated Au-Cu NCs of other sizes, which could further facilitate their application explorations. Synthesis of Au-Cu NCs with improved stability in solution is also of importance in future studies if we would like to use these bi-MNCs for some practical applications.

(c) Au-Pd and Au-Pt NCs

Pd, with an atomic number of 46, and Pt, with an atomic number of 78 are in the VIII group. During the doping of Pd or Pt in Au NCs, they may also cause some incompatibility with Au NCs, such as the lattice mismatch. Unlike Ag, the atomic radii of Pd (1.38 Å) and Pt (1.39 Å) are relatively smaller than that of Au (1.44 Å). Therefore different incorporation patterns may exist in Au-Pd and Au-Pt systems compared to that in the Au-Ag system. Pd and Pt are of importance in many catalytic applications,[36, 95] and the syntheses of Au-Pd and Au-Pt NCs are very attractive in this perspective. Pd and Pt have similar atomic radii and they are in the same VIII group, therefore they may have similar behavior when incorporating with Au NCs. We will discuss the synthesis of Au-Pd and Au-Pt NCs in this subsection.

In 2009, Murray et al. have successfully obtained a mixture of $Au_{25}(SC_2H_4Ph)_{18}$ and $Au_{24}Pd_1(SC_2H_4Ph)_{18}$ NCs via the two-phase Brust method.[30] They observed that only one Pd atom can be doped to Au_{25} NCs regardless of the feeding ratios of Au^{3+}/Pd^{2+}. Interestingly, $Au_{24}Pd_1(SC_2H_4Ph)_{18}$ NCs showed distinctively different optical and electrochemical properties compared to that of $Au_{25}(SC_2H_4Ph)_{18}$ NCs, although there was only one Pd atom difference in these two NCs. In a later study, Negishi et al. and Jin et al. observed that $Au_{24}Pd_1$ NCs were more stable against degradation and laser ablation than Au_{25} NCs. The superior stability of $Au_{24}Pd_1$ NCs could be attributed to its unique core-shell $Pd@Au_{24}(SR)_{18}$ structure, where the central Au atom in the Au_{13} icosahedral core of the Au_{25} NC was replaced by one Pd atom (Figure 1.3a).[73, 81] The unique structure of the $Pd@Au_{24}$ NCs was further confirmed by using ^{197}Au Mossbauer and Pd K-edge extended X-ray absorption fine structure (EXAFS) spectroscopy,[72] which was in good agreement with the theoretical studies; the replacement of the central Au atom by Pd can increase the interaction energy between the central atom and the surrounding $Au_{24}(SR)_{18}$ frame, leading to the formation of the most stable core-shell $Pd@Au_{24}(SR)_{18}$ structure.[84, 93, 96, 97] The increased interaction between the central Pd and the $Au_{24}(SR)_{18}$ frame can improve their ligand-exchange activity, by which the original thiolate ligands on the NC surface can be easily replaced by other thiolate ligands with pre-designed functionalities, leading to the formation of Au-Pd NCs with a tailorable ligand surface.[75]

Similar to the Pd-doped Au NCs, only one Pt atom can be incorporated in $Au_{25}(SC_2H_4Ph)_{18}$ NCs. The Au-Pt NCs also showed improved stability. Both

the experimental and theoretical studies have confirmed that the Pt atom was in the center of Au_{13} icosahedral core (Figure 1.3a).[42, 83] However, it should be noted that no other sized high-quality Au-Pt NCs have been reported so far, possibly due to the challenge in discriminating the atomic mass of Pt from Au, which is only 1.89 Da difference. Therefore, a high-resolution mass spectrometry is required to analyze the formula of Au-Pt NCs.

In a follow-up study, Negishi et al. reported the synthesis and characterizations of $Pd_nAu_{38-n}(SC_2H_4Ph)_{24}$ NCs with the value of n at 1 and 2. They synthesized $Pd_nAu_{38-n}(SC_2H_4Ph)_{24}$ NCs by reducing the metal-thiolate complexes in tetrahydrofuran, followed by separating the as-synthesized $(AuPd)_{38}$ NCs from the $Au_{38}(SC_2H_4Ph)_{24}$ NCs.[78] As shown in Figure 1.3b, this study suggests that the $Pd_2Au_{36}(SC_2H_4Ph)_{24}$ NC has a Pd_2Au_{21} core, where the two Au atoms in the center of the Au_{23} core were replaced by two Pd atoms. This Pd_2Au_{21} core was capped by several Au(I)-SC_2H_4Ph oligomers. Similar to $PdAu_{24}(SR)_{18}$ NCs, $Pd_2Au_{36}(SC_2H_4Ph)_{24}$ NCs also showed higher stability in solution against both degradation and thiol-etching compared to its Au NC analogue, that is $Au_{38}(SR)_{24}$. Very recently, Dass et al. reported the synthesis of $Pd_nAu_{144-n}(SCH_2CH_2Ph)_{60}$ NCs where the number of Pd atoms can be varied by changing the feeding ratios of Au/Pd, and up to 7 Pd atoms can be incorporated in Au NCs.[80] They proposed that the Pd atoms were selectively incorporated in the innermost Au_{12} core.

In addition to the thiolate-protected Au-Pd NCs in solution, naked Au-Pd NCs in gas phase and phosphine-protected Au-Pd NCs in solution have also been studied extensively in the research community.[77, 98, 99] Moreover, many studies have shown the excellent catalytic activities of Au-Pd and Au-Pt

NCs.[41, 42] However, in terms of thiolated Au-Pd and Au-Pt NCs, there are some unresolved issues which may limit their further advances for practical applications. For example, the detailed formation process for Au-Pd and Au-Pt NCs is still not clear. In addition, the electronic and cluster structures of Au-Pd and Au-Pt NCs are unknown, which may constrain both fundamental and applied studies on bi-MNCs. Moreover, systematic investigations of the physicochemical properties of the same sized Au-Ag, Au-Pd, and Au-Pt NCs, are presently lacking. On the other hand, Pd and/or Pt based bi-MNCs incorporated with a few Au and/or Ag atoms are also of importance,[41] and their synthesis and applications could be further explored in the near future.

In summary, one-step or co-reduction method is simple, effective, and versatile in the synthesis of bi-MNCs. It is the most studied method, and a number of bi-MNCs such as Au-Ag, Au-Cu, Au-Pd, and Au-Pt, have been successfully obtained. However, several key issues need to be addressed to further advance this field. For example, the as-synthesized bi-MNCs via the one-step method are hydrophobic because of the usage of hydrophobic thiolate ligands, which may limit their use in the biomedical field where biocompatibility such as water-solubility if is required. Moreover, while all researchers focused on tailoring the composition of metallic cores for gaining maximum multi-functionalities, the identifiably important engineering of the thiolate ligands, which dictates most of the interface-related properties of bi-MNCs, is however not studied. There is therefore a paramount interest in developing facile synthetic strategies for the synthesis of water-soluble bi-MNCs with engineered suface ligand shell, which could further enrich the bi-

MNC family and help fully realize the possible synergistic effects for potential applications.

1.2.2 Two-Step Synthesis of Bi-MNCs

Different from the one-step synthesis of bi-MNCs, where two metal ions are simultaneously reduced in the presence of protecting ligand, two-step synthesis usually involves two steps, where the first step is the preparation of precursors/intermediates such as mono-MNCs and relatively large bi-MNPs, and the second step is the post-treatment of such intermediates/precursors to incorporate the second metal, leading to the formation of bi-MNCs. There are four primary synthetic strategies for bi-MNCs by using a two-step synthesis method. They are galvanic reaction, anti-galvanic reaction, and thiol-etching. It should be noted that the as-synthesized bi-MNCs via the two-step synthesis may have different cluster structures and physicochemical properties when compared to those bi-MNCs prepared by the one-step method. Although the two-step synthesis method requires an additional step compared to the one-step method, the decoupling of two steps for the incorporation of second metals often lead to some interesting physicochemical properties (e.g., luminescence) of the as-synthesized bi-MNCs.

(a) Galvanic Replacement Reaction for the Synthesis of Bi-MNCs

Galvanic replacement is a redox reaction, which can effectively produce metal nanomaterials with controlled compositions and architectures, as demonstrated in many studies in MNP synthesis.[100] The driving force for the galvanic replacement reaction is the redox potential difference between the two metals, where the atoms of one metal ($M_{\#1}$ for short) could be oxidized by

the ions of another metal ($M_{\#2}$) that possesses higher redox potential in solution. Consequently, the metal ions of $M_{\#2}$ are reduced and deposited on the surface of the $M_{\#1}$ template. The galvanic replacement reaction can use a particular metal to reduce a less reactive (or nobler) metal ion in solution. In the noble metal system, mixing Pd, Ag, or Cu NPs with chloroauric acid ($HAuCl_4$) can readily prepare bi-MNPs of Au-Pd, Au-Ag, and Au-Cu, as the redox potential of $AuCl_4^-/Au$ (~1 V) is higher than that of Pd^{2+}/Pd (~0.95 V), Ag^+/Ag (~0.8 V), and Cu^{2+}/Cu (~0.34 V). For example, Ag NPs can be oxidized by $HAuCl_4$ in the reaction solution according to the following redox reaction $3Ag^0 + Au^{3+} \rightarrow Au^0 + 3Ag^+$.[100] This reaction has been well-demonstrated in the synthesis of Au-Ag NPs with controlled morphologies and architectures such as nanocubes and core-shell nanostructures. Of more interest is that the formation kinetics, compositions, and configurations of bi-MNPs could be partially controlled by selecting metal pairs with different redox potentials. The small difference in the redox potentials of metal pairs, such as Au and Pd, makes possible the alloying reaction to proceed in a mild and controlled manner in the reaction solution.

A number of successful attempts have been recently reported. For example, Toshima et al. reported a crown-jewel structured Au-Pd NC by the galvanic replacement reaction.[41] In this study, a Pd_{147} NC was served as the crown, and the Au atoms in the corner of Au-Pd NCs were decorated as jewels, as shown in Figure 1.6. The key to the formation of the Pd crown-Au jewel structured NCs was to apply the surface energy difference of the top, edge, and face Pd atoms of the Pd_{147} NCs, leading to a preferential replacement reaction between Au^{3+} and Pd atoms in the corner. In addition, the slightly

different redox potentials of $AuCl_4^-$/Au (~1 V) and Pd^{2+}/Pd (~0.95 V) also allowed a mild and controlled reaction between Au^{3+} and the corner Pd atoms, making the in situ replacement and deposition possible, particularly in a well-controlled manner.

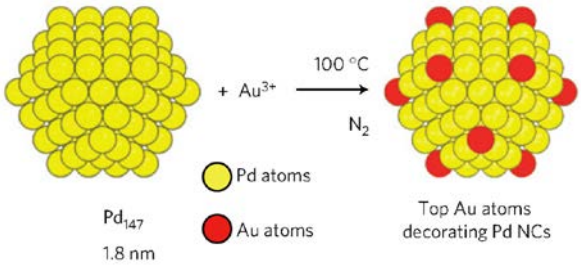

Figure 1.6 Schematic illustration of the synthesis of $(AuPd)_{147}$ NCs by using Au^{3+} to replace the corner Pd atoms in Pd_{147} NCs via the galvanic replacement reaction. Reproduced with permission.[41] Copyright 2011, Nature Publishing Group.

More recently, Pradeep et al. reported several studies in the synthesis of luminescent Au-Ag NCs by using the galvanic replacement reaction. For example, they have successfully synthesized mercaptosuccinic acid (MSA)-protected Ag_7Au_6 NCs by introducing $HAuCl_4$ to a pre-formed MSA-protected $Ag_{7,8}$ NC.[35] The as-synthesized Ag_7Au_6 NCs showed strong red luminescence (at 692 nm) with a quantum yield (QY) of 3.5%. The authors proposed that the thiolate-Au(I) complexes, generated from the reaction of Au^{3+} with the free MSA ligands, reacted with the $Ag_{7,8}$ NCs, leading to the formation of Au-Ag NCs. However, why and how the 6 Au atoms were attached to the $Ag_{7,8}$ NC template to form Ag_7Au_6 NCs in the reaction solution, are still unclear, which require future efforts to systematically study the formation process of Au-Ag NCs during the galvanic replacement reaction.[101] More recently, luminescent protein-protected Au-Ag NCs have also been prepared by mixing Au^{3+} ions with a pre-formed protein-protected Ag NC.[48]

The authors used bovine serum albumin (BSA) as the protecting ligand, and successfully prepared BSA-protected Ag_{31} NCs. A series of red-emitting Au-Ag NCs with different compositions have been synthesized by introducing different amount of Au^{3+} ions in the BSA-protected Ag_{31} NCs. Another example is the solid grinding method for the synthesis of protein-protected Au-Ag NCs.[102]

The galvanic replacement reaction is a powerful, versatile, and straightforward method for the synthesis of bi-MNCs.[35, 41, 44, 48, 101, 102] With continuous efforts from the research community, by using the galvanic replacement reaction, a large number of new bi-MNC species with well-controlled compositions, structures, and surface chemistries could be obtained, which may further promote their applications in catalysis, bioimaging, and sensing.

(b) Anti-Galvanic Replacement Reaction for the Synthesis of Bi-MNCs

According to the galvanic replacement reaction principle, the Au ion can oxidize the metallic Ag atom due to its higher redox potential, which also indicates that the reverse reaction (the oxidation of metallic Au by Ag ions) is not thermodynamically favorable. This principle may not work when the sizes of MNPs decrease to below 2 nm. For example, recently, Wu et al. observed a very interesting anti-galvanic replacement reaction in MNCs, where metal ions (e.g., Ag) were reduced by a more noble metal Au.[50] In particular, as shown in Figure 1.7, the authors mixed the $Au_{25}(SC_2H_4Ph)_{18}$ NCs and a certain amount of Ag^+ ions, and observed that several bi-MNC species such as $Au_{22}Ag_3$ and $Au_{23}Ag_2$ were formed. This data suggests that Ag^+ ions have replaced the Au atoms in the Au_{25} NCs. This interesting observation was further confirmed by

using other Au NPs with core sizes of 2-3 nm as the parental NPs. In addition, the authors also demonstrated that the anti-galvanic replacement reaction was also applicable to other metal pairs such as Ag-Cu, where Cu^{2+} ions were reduced and incorporated in the HSC_2H_4Ph-protected Ag NPs (~3 nm in core size). Very recently, Li et al. showed that the anti-galvanic replacement reaction also worked for Au NCs protected by DNA.[49]

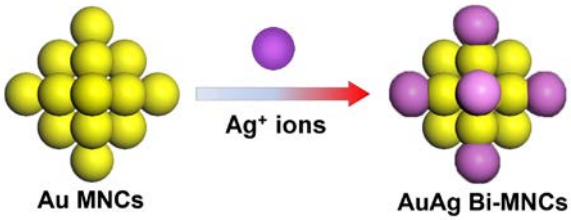

Figure 1.7 Schematic illustration of the synthesis of Au-Ag NCs by using Ag^+ ions to replace Au atoms in Au NCs via the anti-galvanic replacement reaction.

Although the phenomenon of anti-galvanic replacement reaction has been observed, the underlying chemistry of this reaction in the NC system is presently unclear. In addition, it should be mentioned that the anti-galvanic replacement reaction could also be affected by the protecting ligands. For example, if a bio-thiol ligand, such as glutathione (GSH) was chosen as the protecting ligand for Au_{25} NCs, the Au atoms in $Au_{25}(GSH)_{18}$ NCs could not be replaced by the Ag^+ ions introduced to the solution.[103] Therefore, more systematically experimental and theoretical studies are required to further understand the underlying chemistry of the anti-galvanic replacement reaction for the bi-MNC formation.

(c) Thiol-Etching of bi-MNPs for the Synthesis of Bi-MNCs

Another strategy for synthesizing bi-MNCs is to use thiolate ligands as etchants to digest the relatively large-sized bi-MNPs. This method relies on

the strong interaction between thiolate ligands and Au/Ag atoms. The introduction of excess thiolate ligands could digest the relatively large-sized bi-MNPs, leading to the formation of smaller-sized bi-MNCs (Figure 1.8). In general, the thiol-etching method can obtain bi-MNCs that copy the composition of their parental bi-MNPs. Therefore, the composition control of bi-MNCs via the thiol-etching method was usually achieved during the preparation of bi-MNPs. While the thiol-etching method has been widely used to synthesize mono-MNCs, the synthesis of bi-MNCs by using this method is much less attempted in the research community.

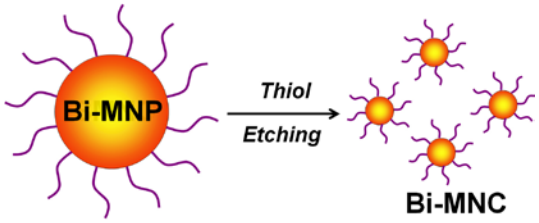

Figure 1.8 Schematic illustration of the thiol-etching method for the synthesis of bi-MNCs

One successful demonstration was recently reported by Chang et al.[51] They first prepared a series of Au-Ag NPs with core sizes of ~2.6 nm. These Au-Ag NPs were protected by tetrakis(hydroxymethyl)phosphonium chloride (THPC), and with adjustable ratios of Au to Ag. Thereafter, a thiolate ligand, 11-mercaptoundecanoic acid (MUA), was introduced to digest the as-prepared THPC-protected Au-Ag NPs, leading to the formation of MUA-protected Au-Ag NCs with an average size of ~1.7 nm. Another interesting finding in this study was that the luminescence color can be tuned by increasing the Ag content in the as-synthesized Au-Ag NCs.[51]

Thiol-etching provides an efficient way to prepare luminescent Au-Ag NCs. Further studies in this direction may need to develop more efficient methods to prepare the parental Au-Ag NPs with good control of sizes,

compositions, and structures, which could subsequently lead to the formation of Au-Ag NCs with an improved quality. Some fundamental issues related to the etching process, such as the underlying chemistry for the thiol-etching and the formation mechanism for the Au-Ag NCs, may also require to be addressed to further advance this field.

1.3 Applications of Bi-MNCs

The incorporation of two metals in one particle combines the physicochemical properties of two metals, which often generate some synergistic properties of the as-synthesized bi-MNCs, some of which are difficult or impossible to be realized in their mono-MNC analogues. The unique or improved physicochemical properties of bi-MNCs have facilitated their applications in diverse fields like catalysis, sensing, and bioimaging. Here we will only illustrate some examples, demonstrating that the unique electronic structures and strong luminescence of bi-MNCs can be readily used for applications such as catalysis, sensing, and bioimaging.

1.3.1 Catalysis

Recently, bimetallic nanomaterials (e.g., ? NPs) have emerged as a promising class of catalysts for a variety of chemical reactions. In many cases, bi-MNPs may show higher catalytic efficiency compared to their monometallic counterparts, most likely because of the strong synergistic effects of two integrated metals in one particle. In comparison with bi-MNPs, bi-MNCs are much smaller (typically consisting of several to tens of metal atoms), and they are more sensitive to the incorporation of foreign metals; for instance, only one foreign metal atom doping may cause a remarkable

difference in the cluster structure and physicochemical properties of bi-MNCs. Bi-MNCs with well-controlled particle sizes (atomically precise), compositions (at atomic level), and structures, are promising models for some catalytic reactions, which have been extensively studied in the research community.

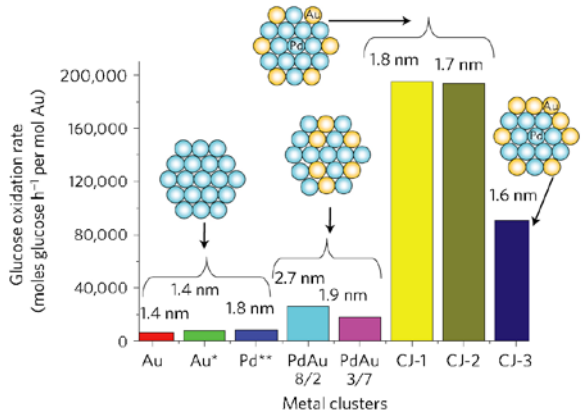

Figure 1.9 Comparison of the catalytic activity of the crown-jewel structured Pd-Au NCs, alloyed Pd-Au NCs, Au NCs, and Pd NCs for the aerobic glucose oxidation. The insets and numbers are the cartoon structures and the average particle sizes of the NCs, respectively. Reproduced with permission.[41] Copyright 2011, Nature Publishing Group.

For example, Toshima et al. prepared a Pd crown-Au jewel structured bi-MNC via the galvanic replacement reaction. They have applied the as-prepared Au-Pd NCs as catalysts for the aerobic glucose oxidation.[41] As shown in Figure 1.9, compared to Au, Pd, and alloyed Au-Pd NCs, the unique Pd crown-Au jewel structured NCs showed much higher catalytic activity. The excellent activity of Pd crown-Au jewel NCs was attributed to 1) the Au atoms in the corner of Pd_{147} NCs have a higher degree of coordinative unsaturation, and they are more active for the chemical reactions; 2) the corner Au atoms that are surrounded by several Pd atoms may show higher activity in some catalytic reaction systems as the activity of catalytic surface is often improved by the neighboring hetero-metals. This study clearly showed that the

properties of bi-MNCs could be efficiently tailored by the architectural design, providing new ways to design better bi-MNC catalysts.

Many of the exciting findings in this field have shown that bi-MNCs are promising catalysts for a diverse spectrum of reactions. Some issues need to be addressed in future studies. For example, most of the catalytic examples of bi-MNCs were related to the oxidation reactions.[47, 71, 104, 105] Continuous efforts are required to explore the applications of bi-MNCs for other reactions, such as reduction, dehydrogenation, Suzuki, and Heck cross-coupling.[95, 106] In addition, to further advance bi-MNCs for practical catalytic reactions, the stability and durability of as-prepared bi-MNC-based catalysts need to be improved. This issue has been partially addressed by depositing the as-prepared bi-MNCs on some inorganic substrates, such as TiO_2, Al_2O_3, and mesoporous nanomaterials.[107-109]

1.3.2 Sensor Development

Optical sensors have attracted increasing interest due to their promising applications in environmental monitoring, molecular recognition, and biomedical diagnosis. In a typical optical sensor, an optical probe is an indispensible component, and the choice of the optical probes may dictate their sensing performance. In the past two decades, organic dyes, quantum dots, noble metal NPs, and ultrasmall MNCs have been used as optical probes for a variety of sensor developments. Among these newly-developed optical probes, highly luminescent MNCs are attractive due to their excellent optical properties and ultrasmall sizes, leading to an improved sensor performance in terms of simplicity (in both sensor construction and operation), high selectivity and sensitivity, and miniaturizability. While luminescent mono-

MNCs are recently used to construct sensors for a variety of analytes, such as toxic metal cations, anions, and biomolecules, only very few examples have been reported for the luminescent bi-MNCs. Some nice demonstrations exist. For example, Zhou et al. recently developed a NC-based optical probe for Al^{3+} ion detection. They used poly(ethylene glycol) (PEG) grafted MSA-protected luminescent Au-Ag NCs as the recognition component, and the developed optical sensor displayed high selectivity and excellent sensitivity (detection limit of 0.8 μM) for Al^{3+} ions based on luminescence enhancement in aqueous solution. Authors proposed that the signal-generation mechanism for Al^{3+} ion detection was possibly due to the deposition of Al^{3+} ions on the surface of the metal core.[44] In addition, luminescent Au-Ag NCs protected by BSA have been used to detect Cu^{2+} ions, showing an excellent selectivity.[110]

To date, only luminescent bi-MNCs have been used for sensor development. Other interesting synergistic properties, such as strong catalytic activity, unique and tailorable metal-analyte interaction, and the steric hindrance of the organic ligand layer, could be further explored for sensor developments in future.

1.3.3 Bioimaging

Ultrasmall luminescent bi-MNCs feature with strong luminescence, good biocompatibility, and excellent photo and chemical stability in solution, which made them attractive for a variety of bioimaging applications. There are several successful demonstrations recently. For example, Schneider et al. prepared highly luminescent GSH-protected Au-Ag NCs, showing strong red emission at 615 nm (Figure 1.10a).[43] The intriguing properties of the as-synthesized GSH-protected Au-Ag NCs, such as strong luminescence,

biocompatable organic ligand, and ultrasmall size, have motivated the development of the Au-Ag NCs for bioimaging. Owing to the good biocompatibility of the GSH ligand, and a small amount of reduced Ag in the as-prepared Au-Ag NCs, no obvious cytotoxicity was observed after 4 h of incubation with the Au-Ag NCs. As shown in Figure 1.10b, the red-emitting Au-Ag NCs were easily seen inside the lung cancer cells A549. These NCs were found in the cytosol rather than in the nucleus of the cells. Transmission electron microscopy (TEM) images showed that the Au-Ag NCs were inside some vesicles (Figure 1.10c), indicating the involvement of an endocytosis-like uptake. This study clearly supports the great potential of highly luminescent Au-Ag NCs for live cell imaging. More recently, Wang et al. also demonstrated the labelling of living cells (human cancer cell 7402) by using highly luminescent Au-Ag NCs protected by phosphine and hydroxyethylthiol ligands.[111] Continuous efforts in this field may further pave their way towards the in vivo bioimaging.

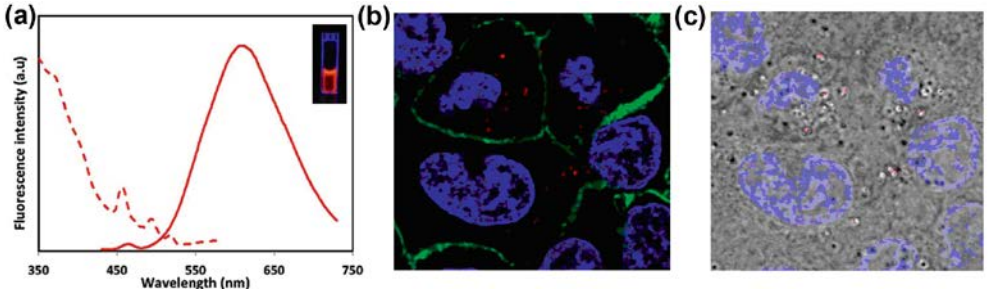

Figure 1.10 (a) Photoexcitation (dashed line), photoemission (solid line) spectra, and digital photograph (inset) of the as-synthesized luminescent GSH-protected Au-Ag NCs. (b) Representative luminescent and TEM images of the GSH-protected Au-Ag NCs in lung cancer cells (A549) after 4 h of incubation. The cell membrane was stained with FITC (green) and the nuclei was stained with DAPI (blue). Reproduced with permission.[43] Copyright 2012, Royal Society of Chemistry.

1.4 Research Gaps and Objectives

The results of literature review clearly suggested that the high-quality bi-MNCs are an emerging class of multi-functional nanomaterials. A number of good synthesis methods have been recently developed for high-quality bi-MNCs with well-defined sizes, compositions, and structures. Among them, One-step synthesis or co-reduction method is facile and efficient for the synthesis of monodisperse bi-MNCs with well-controlled sizes, and compositions. In contrast, the two-step synthesis method often produces luminescent bi-MNCs. The two metal species integrated in one bi-MNC show some interesting synergistic properties, such as tunable electronic structures and luminescence. Such properties have rapidly motivated the research community to use bi-MNCs in many applications such as catalysis, sensing, and bioimaging. Despite the substantial progress in the synthesis and applications of bi-MNCs in recent years, there are several key issues that still need to be addressed.

Firstly, while hydrophobic bi-MNCs have been extensively studied, investigations of high-quality hydrophilic bi-MNCs are very rare. Furthermore, all previous studies focused on tailoring the compositions of metallic core, and there is no successful attempt in engineering the surface chemistry of bi-MNC's ligand shell, although it is well documented that most of interface-related properties of nanomaterials are dictated by the functionalities of their surface thiolate ligands. The lacking of studies in such aspects may largely affect the advances of bi-MNCs in biomedical applications. There is therefore of significant interest in developing efficient synthesis methods for the preparation of high-quality hydrophilic bi-MNCs with both controllable

metallic compositions and adjustable surface ligand chemistry, especially those protocols that can produce quantities large enough for application explorations.

In addition, most of the reported bi-MNCs showed very weak luminescence, and the corresponding luminescence mechanism is still unclear, which may limit their use as luminescent probes for sensing and bioimaging applications, especially those applied in the in vivo settings. There is a pressing need to develop efficient methods for highly luminescent bi-MNCs with a deep understanding of their luminescence mechanism.

As such, this mater thesis is focused on developing new strategies to synthesize water-soluble bi-MNCs with controllable metallic compositions/surface ligand chemistry, or high luminescence. The specific objectives are listed as follows:

1. Develop a general protocol to synthesize water-soluble AuAg bi-MNCs protected by mono- and bi-thiolate ligands with tunable metallic compositions as well as rich surface functionalities (e.g., carboxyl, hydroxyl, and amine groups).

2. Develop a facial method to synthesize water-soluble and highly luminescent AuAg bi-MNCs, and understand the underlying luminescence mechanism of the as-synthesized bi-MNCs.

Through this master project, it is anticipated that a series of high-quality water-soluble AuAg bi-MNCs with either tunable metallic compositions/surface ligand functionalities or high luminescence could be

synthesized. In addition, the underlying luminescent mechanism of the bi-MNCs could be clearly clarified.

1.5 Thesis Outline

This thesis consists of four chapters. As can be seen Chapter 1 describes the general research background, the progress of bi-MNCs in literatures, research gaps and objectives of this project, as well as the thesis outline. In Chapter 2, a general strategy to synthesize water-soluble AuAg bi-MNCs with tunable metallic compositions/surface ligand functionalities is developed. Chapter 3 presents a facile approach to prepare water-soluble and highly luminescent AuAg bi-MNCs. The underlying luminescence mechanism of the bi-MNCs is also investigated. Chapter 4 summarizes the conclusions of this thesis and future research directions are recommended.

CHAPTER 2 FACILE SYNTHESIS OF WATER-SOLUBLE BIMETALLIC $(AuAg)_{25}$ NANOCLUSTERS PROTECTED BY MONO- AND BI-THIOLATE LIGANDS

2.1 Introduction

Noble metal nanoparticles (MNPs) have attracted recent interest due to their applications in many fields of catalysis, sensing, bioimaging, drug delivery and therapy.[3, 17, 19, 20, 26, 112-114] MNPs contain a metal core and a ligand shell, and their physicochemical properties can be readily tailored either by controlling the attributes of their metal core, such as size, shape, and composition,[37, 38, 106, 115] or by modifying the ligand such as surface charge, functional group, and structure.[116-118] There are two efficient ways that can produce metal MNPs with multi-functionalities, which are 1)integrating two or more metal species into one single MNP, leading to the formation of bi-or multi-metallic MNPs; and 2) integrating two or more protecting ligands on the surface of metal NPs, resulting mixed-ligand-protected metal MNPs with good control of surface properties.[106, 116-119] The key challenge in obtaining bi-metallic NPs is the redox potential difference of the metal pairs (e.g., $AuCl_4^-$ /Au of ~1.0 V and Ag^+/Ag of ~0.8 V), which could lead to the phase separation of two MNPs in the same reaction solution.[88] Similarly, the phase separation of hetero-ligands on the NP surface is also a key issue in producing mixed-ligand-protected MNPs, most likely due to the different reactivities of ligand pairs towards the metal surface.[117, 120, 121] It would be even more

challenging to integrate both hetero-metals and hetero-ligands into one MNP to form mixed-ligand-protected bi-metallic NPs, which may have more intriguing physical and chemical properties compared to their mono-metallic or mono-ligand-protected analogues. Therefore, it is of paramount interest in developing efficient methods to produce bi-metallic NPs protected by mixed-ligands, which is an account of this study.

In this chapter, we develop a facile yet efficient synthesis method to produce water-soluble AuAg MNPs protected by bi-thiolate ligands with good control of both the metal core (size and composition with atomic precision) and ligand surface (various ligand combinations and ratios of two ligands). The key strategy is to use the different affinity of thiolate ligands with Au and Ag, (than that of Ag-thiolate) to mitigate their redox potentials difference, leading to a simultaneous reduction of Au^{3+} and Ag^{+} to form AuAg NPs with well-controlled sizes and compositions.[122] In addition, mixed-thiolate-protected AuAg NPs with adjustable ratios of thiolate ligands can also be easily obtained, which could further enrich the surface functionalities of NPs and facilitate their interface-related applications such as catalysis and biomedicine.[19, 119, 123]

Our target materials are ultrasmall AuAg MNPs with core sizes below < 2 nm, which are typically referred to as MNCs.[2, 6, 27, 45, 46] MNCs, typically consisting of several to a hundred metal atoms, show discrete and size-dependent electronic transitions due to the strong quantum confinement effects in this size regime.[5, 16, 124] In such ultrasmall MNCs, doping of only one foreign metal in the NCs may result in remarkable changes of their electronic and geometric structures.[42, 73] Therefore doping a certain number of foreign

metal atoms in the MNCs is an effective way to study the composition-/structure-properties correlations, such as optical and catalysis properties.[42, 75] There are two primary approaches to produce AuAg NCs. The first approach is one-step or co-reduction method, where Au and Ag precursors (e.g., $HAuCl_4$ and $AgNO_3$) were co-reduced in the presence of a particular thiolate ligand.[31-33, 40, 79, 82] The second approach is two-step method, where a typical Au or Ag precursors were first prepared, followed by an incorporation of Ag or Au in the MNC to form a AuAg NC.[34, 35, 50] Among these synthetic approaches, the co-reduction method is the most facile and efficient, and it has been well-demonstrated recently to produce AuAg NCs protected by hydrophobic thiolate ligands. However, the synthesis of AuAg NCs protected by water-soluble thiolate ligands still remains as grand challenge, not to say those AuAg NCs protected by mixed-thiolate-ligands in water.[19, 123]

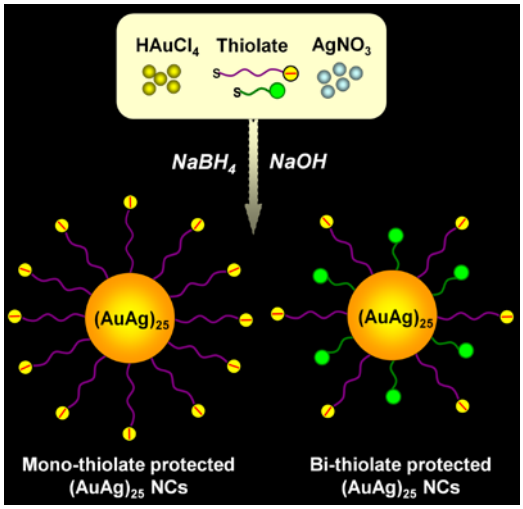

Figure 2.1 Schematic illustration of the synthetic process of mono- and bi-thiolate-protected $(AuAg)_{25}$ NCs via NaOH-mediated $NaBH_4$ reduction method.

The synthesis of water-soluble mono- and bi-thiolate-protected bimetallic AuAg NCs from our recently developed "NaOH-mediated $NaBH_4$ reduction method".[125] As shown in Figure 2.1, this is a very simple one-step co-

reduction method, where aqueous solutions of $HAuCl_4$, $AgNO_3$, and hydrophilic thiolate ligands were first mixed to form thiolate-Au(I)/Ag(I) complexes, followed by the addition of $NaBH_4$ to reduce the thiolate-complexes, leading to the formation of mono-thiolate-protected $(AuAg)_{25}$ NCs with various ligand combinations, such as thiolate ligands with carboxyl, amine, and hydroxyl groups, can be easily obtained. Our protocol is facile, fast (≤3 h), and versatile (applicable for various thiolate ligands), and can produce high-quality $(AuAg)_{25}$ NCs in water. Moreover, the proportions of both the Au and Ag in the metal core, and hetero-thiolate ligands on the NC surface, can be continuously tuned by simply varying the feeding ratios of metal precursors or hetero-thiolate ligands.

2.2 Experimental Section

2.2.1 Materials

Ultrapure water (18.2 MΩ) was used in this study. All glassware and magnetic stir bars were washed with *aqua regia*, rinsed with abundant ethanol and ultrapure water. Hydrogen tetrachloroaurate (III) hydrate ($HAuCl_4 \cdot 3H_2O$) from Alfa Aesar; sodium hydroxide (NaOH) and silver nitrate ($AgNO_3$) from Merck; 6-mercaptohexanoic acid (MHA), 8-mercaptooctanoic acid (MOA), 11-Mercaptoundecanoic acid (MUA), cysteamine hydrocholoride (Cystm), 2-mercaptoethanol (MetH), and Sodium borohydride ($NaBH_4$), from Sigma-Aldrich; were used as received.

2.2.2 Characterization

Optical UV-vis spectra were recorded on a Shimadzu UV-1800 spectrometer. The mass of bimetallic AuAg NCs were determined by

electrospray ionization (ESI) mass spectrometry on a Bruker microTOF-Q system. Transmission electron microscopy (TEM) images were obtained on a JEOL JEM 2010 microscope operating at 200 kV. X-ray photoelectron spectroscopy (XPS) was conducted on a Kratos AXIS Ultra^{DLD} spectrometer.

2.2.3 Synthesis of Mono-Thiolate Protected $(AuAg)_{25}$ NCs

Mono-thiolate protected $(AuAg)_{25}$ NCs were synthesized according to our previously developed NaOH-mediated $NaBH_4$ reduction method. In a typical experiment to synthesize MHA-$(AuAg)_{25}$ NCs, aqueous solution of MHA (5 mM, 2 mL) were first mixed in water (2.35 mL), followed by the introduction of a mixing solution (0.25 mL) of $HAuCl_4$ (20 mM) and $AgNO_3$ (20 mM) with different ratios ($R_{Au/Ag}$ = 24:1, 22:3, 18:7, 16:9, and 14: 11), leading to the formation of MHA-Au(I)/Ag(I) complexes under stirring condition. Here thiol ligands could reduce Au(III) to Au(I) via the formation of disulfide bond (S-S bond).[126] NaOH solution (1 M, 0.3 mL) and $NaBH_4$ solution (~112 mM, 0.1 mL, prepared by dissolving 43 mg of $NaBH_4$ powder in NaOH solution (10 mL, 0.2 M)) were then separately added into the reaction mixture. The MHA-$(AuAg)_{25}$ NCs were collected after stirring of 3 hrs for further characterizations. A series of MHA-$(AuAg)_{25}$ NCs synthesized under the condition of different feeding $R_{Au/Ag}$ are referred to as NC 1-5. Varying the volume of NaOH solution from 0.3 mL to 0.08 mL while keeping the other synthetic conditions unchanged, $(AuAg)_{25}(MOA)_{18}$ and $(AuAg)_{25}(MUA)_{18}$ NCs could be synthesized. Here it should be mentioned that the MUA ligand was dissolved in ethanol.

2.2.4 Synthesis of Bi-Thiolate Protected $(AuAg)_{25}$ NCs

Bi-thiolate protected $(AuAg)_{25}$ NCs can be synthesized by keeping all the experimental conditions unchanged except for the introduction of the second thiolate ligand. Typically, keep the total volume of thiolates to be 2 mL, and gradually adjust amount of MHA (from 1.75, 1.5, 1.25, to 1 mL) and MetH (from 0.25, 0.5, 0.75, to 1 mL), $(AuAg)_{25}$ NCs protected by MHA and MetH with different ligand and/or metal proportions can be obtained. The synthesis of bi-thiolate protected $(AuAg)_{25}(MHA/Cystm)_{18}$ NCs can also be achieved by using the same strategy.

2.3 Results and Discussion

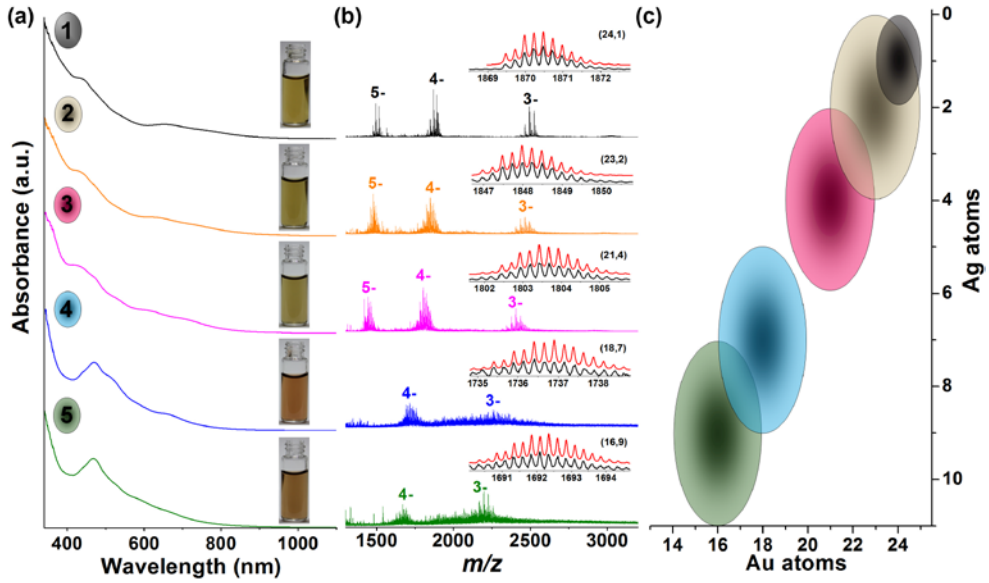

Figure 2.2 (a) UV-vis absorption, (b) ESI mass spectra (in negative ion mode), and (c) compositional distributions of the as-synthesized MHA-protected $(AuAg)_{25}$ NC 1-5. Insets in Figure 2.2a show photographs of corresponding NC samples; insets in Figure 2.2b show theoretically simulated (red lines) and experimentally acquired (black lines) isotope patterns of middle species in corresponding NCs. Figure 2.2c shows that the obtained MHA-$(AuAg)_{25}$ NCs have evolved distributions of metallic compositions: NC-1 (Au/Ag= 23:2—25:0); NC-2 (Au/Ag= 21:4—25:0); NC-3 (Au/Ag= 19:6—23:2); NC-4 (Au/Ag= 16:9—20:5; NC 5 (Au/Ag= 14:11—18:7).

As a proof of concept, 6-mercaptohexanoic acid (MHA) was chosen as our model ligand. Five different feeding ratios of Au^{3+}/Ag^{+} or $R_{Au/Ag}$ ($R_{Au/Ag}$ = 24:1, 22:3, 18:7, 16:9, and 14: 11) were used to synthesize MHA-protected $(AuAg)_{25}$ NCs. A series of MHA-protected AuAg NCs were collected after 3 h, which were referred to as **NC 1-5**, according to their different $R_{Au/Ag}$ [NC-1 ($R_{Au/Ag}$=24/1); NC-2 ($R_{Au/Ag}$=22/3); NC-3 ($R_{Au/Ag}$=18/7); NC-4 ($R_{Au/Ag}$=16/9); NC-5 ($R_{Au/Ag}$=14/11)]. The as-synthesized NC 1-5 were first examined by UV−vis spectroscopy. As shown in Figure 2.2a, **NC-1 and NC-2** displayed four distinct absorption peaks at 440, 552, 670, and 760 nm (black and brown lines), which match nicely with the characteristic optical absorptions of thiolate-protected Au_{25} NCs (Figure 2.3a).[59] The well-structured absorption spectra of NC 1-2 suggest that the as-synthesized $(AuAg)_{25}$ NCs may feature with the same cluster structure as Au_{25} NCs. Interestingly, a further decrease of the feeding ratios $R_{Au/Ag,}$ such as to 18/7 (**NC-3**), 16/9 (**NC-4**), and 14/11 (**NC-5**), resulted in the formation of AuAg NCs with different UV-vis absorptions compared to that of Au_{25} NCs. For example, a weak absorption peak at ~470 nm was observed for **NC-3** (pink line in Figure 2.2a), which was evolved to more distinct in the absorption spectra of **NC-4** and **NC-5** (blue and green lines). The absorption feature evolutions were also reflected in their solution colors, from brown for NC-3 to reddish-brown for NC-4 and NC-5 (insets of Figure 2.2a). The differences in the optical absorptions and solution colors of NC 1-5 were most likely due to the continuous incorporation of Ag in the Au NCs, possibly with a continuous increase of Ag atoms in AuAg NCs from NC-1 to NC-5.

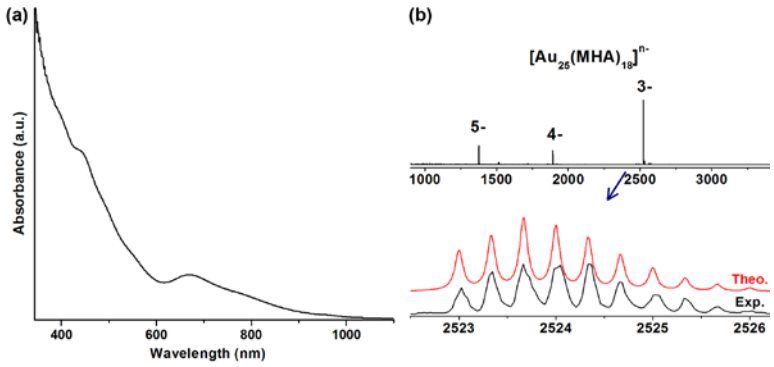

Figure 2.3 (a) UV-vis absorption spectrum and (b) ESI mass spectra of the as-synthesized MHA-protected Au_{25} NCs. The lower panel in (b) shows isotope patterns of $[Au_{25}(MHA)_{18}\text{-}2H]^{3-}$ acquired theoretically (red) and experimentally (black).

The molecular formulas of the as-synthesized AuAg NCs were determined by electrospray ionization (ESI) mass spectrometry. For example, for NC-1, we observed three sets of intense peaks at ~m/z 1495, 1868, and 2492 in the range of 1200−3300 (Figure 2.2b, black line), which can be assigned to $(AuAg)_{25}$ NCs carrying 5-, 4-, and 3- charges, respectively. These assignments were supported by the good agreements of the representative isotope patterns acquired experimentally and theoretically (inset of Figure 2.2b). In addition, the ESI-MS data clearly suggested that NC-1 was a mixture of $Au_{23}Ag_2(MHA)_{18}$, $Au_{24}Ag_1(MHA)_{18}$, and $Au_{25}Ag_0(MHA)_{18}$ (Figure 2.2c, black retangle). Figure 2.4a presents the detailed ESI-MS analysis of NC-1. With a decrease of the feeding ratio $R_{Au/Ag}$, the ESI-MS peaks gradually shifted to lower *m/z* (Figure 2.2b), implying that more Ag atoms have been doped in the Au NCs as the atomic mass of Ag is lower than Au. This conclusion has been further confirmed by their isotope patterns (insets of Figure 2.2b). The detailed analysis of the ESI-MS of NC 2-5 suggest that they were $Au_{21\text{-}25}Ag_{4\text{-}0}(MHA)_{18}$ (NC-2, light brown area), $Au_{19\text{-}23}Ag_{6\text{-}2}(MHA)_{18}$ (NC-3, pink area), $Au_{16\text{-}20}Ag_{9\text{-}5}(MHA)_{18}$ (NC-4, blue area), and $Au_{14\text{-}18}Ag_{11\text{-}7}(MHA)_{18}$ (NC-5, green area). Figure 2.4b-e represents the detailed analysis of ESI-MS of NC 2-

5. In addition, the representative transmission electron microscopy (TEM) images (Figure 2.5) suggest that the as-synthesized $(AuAg)_{25}(MHA)_{18}$ NCs in NC 1-5 all had size below 1.5 nm, similar to the size of $Au_{25}(MHA)_{18}$ NCs (Figure 2.6).

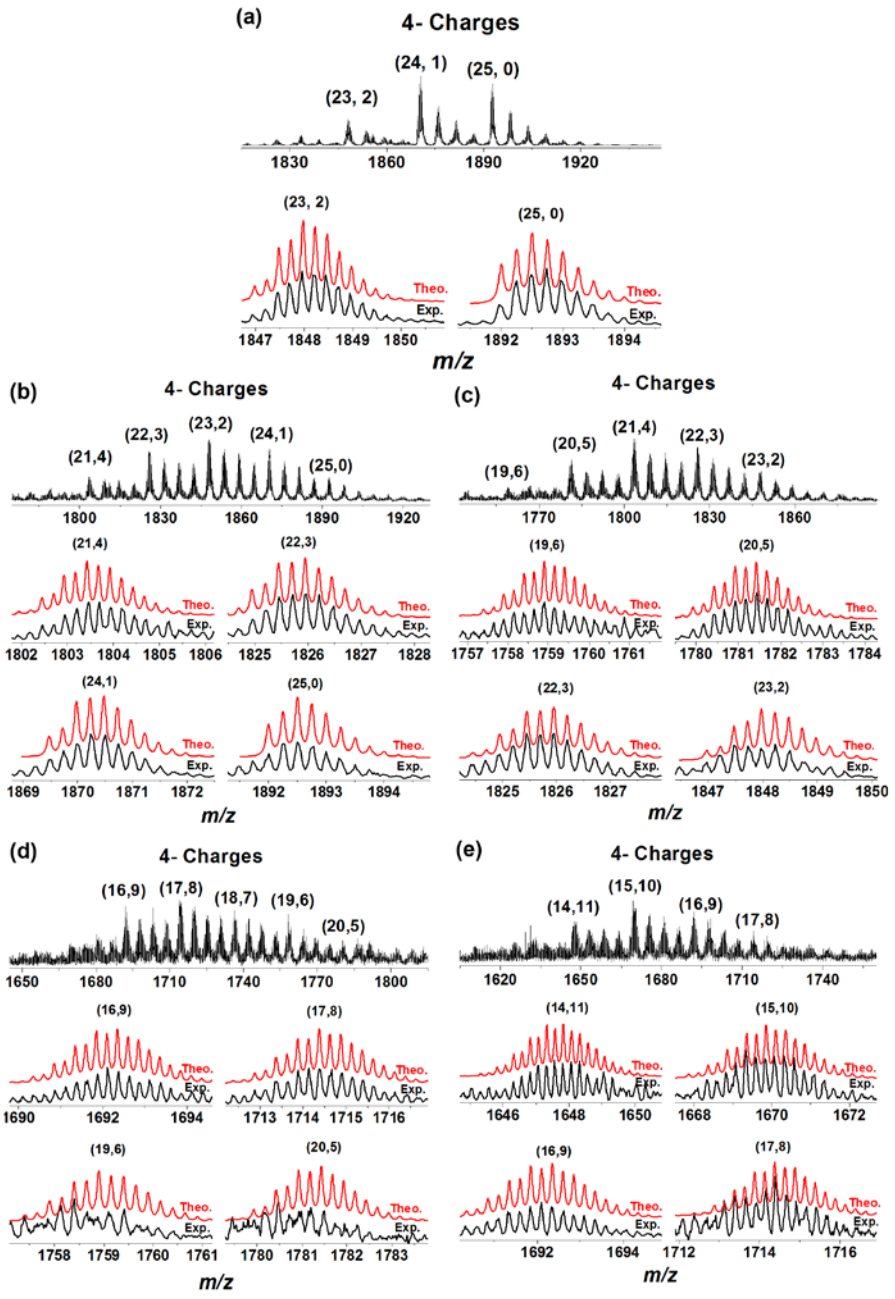

Figure 2.4 Zoom-in ESI mass spectra and representative isotope patterns (theoretical / red and experimental / black) of 4- charged MHA-protected $(AuAg)_{25}$ NCs: (a) **NC-1**, (b) **NC-2**, (c) **NC-3**, (d) **NC-4**, and (e) **NC-5**. The numbers within the bracket are the number of Au and Ag atoms in $(AuAg)_{25}$ NCs. For example, (21,4) is denoted as $Au_{21}Ag_4$ NC species.

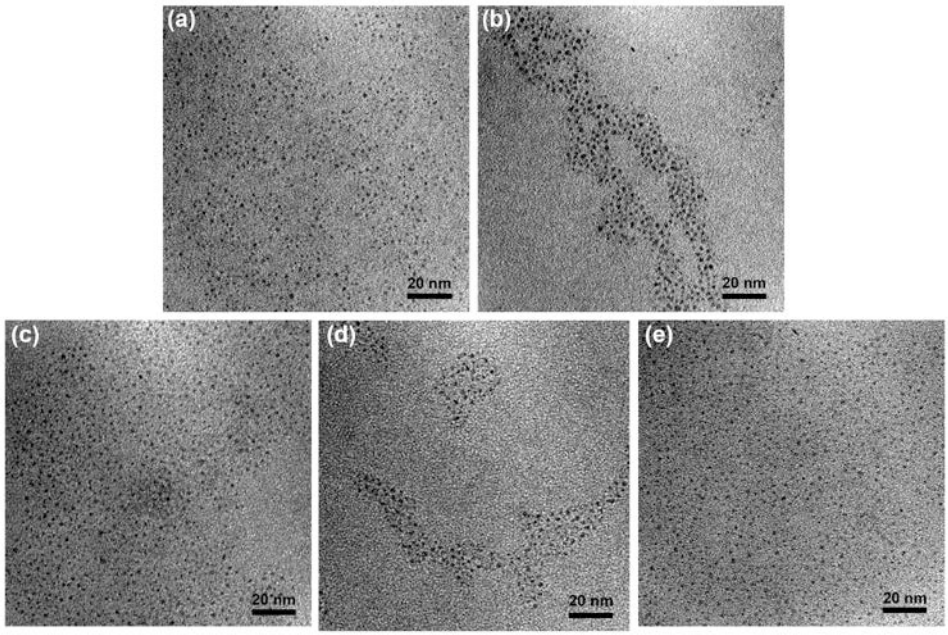

Figure 2.5 Representative TEM images of the as-synthesized MHA-protected $(AuAg)_{25}$ NCs: NC-1 (a), NC-2 (b), NC-3 (c), NC-4 (d), and NC-5 (e).

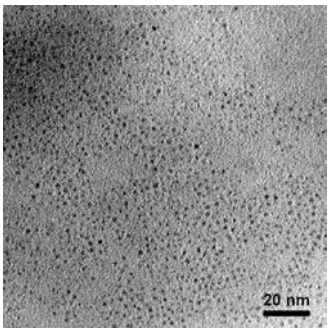

Figure 2.6 A representative TEM image of the as-synthesized $Au_{25}(MHA)_{18}$ NCs.

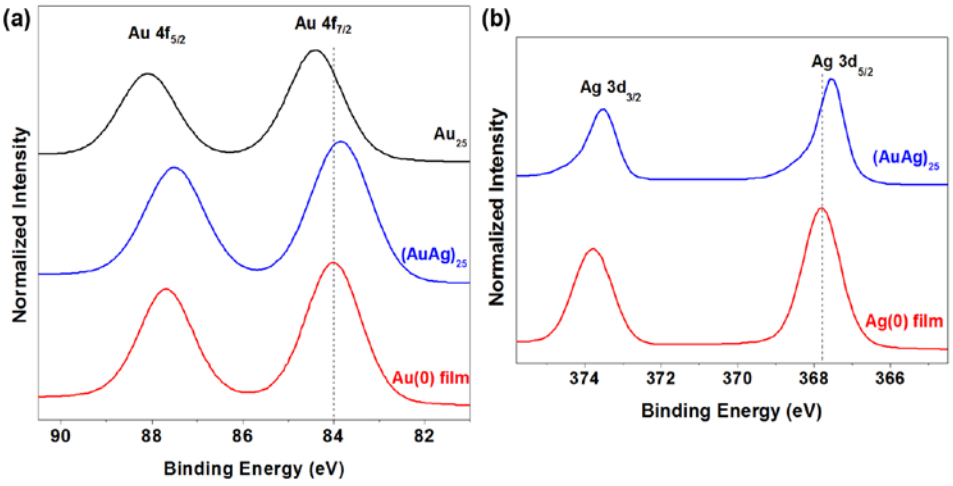

Figure 2.7 XPS spectra of (a) Au 4f species of MHA-protected Au_{25}, MHA-protected $(AuAg)_{25}$ NCs, and Au(0) film, and (b) Ag 3d species of MHA-protected $(AuAg)_{25}$ NCs, and Ag(0) film.

Au and Ag have a similar atomic radius of 1.44 Å,[74] and Ag atoms can be easily incorporated with Au atoms to form AuAg NCs. The next question we may ask is where these Ag atoms located in the AuAg NCs are. It is well-documented that thiolate-protected Au_{25} NCs feature with a core-shell structure with an icosahedral Au_{13} core surrounded by an outer shell of Au_{12}.[11, 58] Ag atoms in the bimetallic NCs could exist in the M_{13} core, outer M_{12} shell, or both. We speculated that all the Ag atoms in our $(AuAg)_{25}$ NCs (up to 11 Ag atoms doped in our system) are located in the M_{13} core rather than in the M_{12} shell, according to the following experimental evidences: (1) This hypothesis was supported by X-ray photoelectron spectroscopy (XPS) analysis of the as-synthesized $(AuAg)_{25}$ NCs. Taking NC-2 $[Au_{21-25}Ag_{4-0}(MHA)_{18}]$ as an example (Figure 2.7), the binding energy of Au $4f_{7/2}$ species in NC 2 (83.85 eV, blue line) is lower than that of Au(0) film (84 eV, Figure 2.7a, red line) and $Au_{25}(MHA)_{18}$ NCs (84.4 eV, Figure 2.7a, black line), implying that the Au atoms in NC-2 were not only reduced by $NaBH_4$ but also carried some negative charges. By comparison, the binding energy of Ag 3d species in NC 2 (367.57 eV; Figure 2.7b, blue line) was lower than that of Ag(0) (367.7 eV; Figure 2.7b red line), indicating that the Ag atoms in NC-2 were positively charged.[31, 82] These results reveal that there were some charge transfers from Ag (electronegativity = 1.93) to Au (electronegativity = 2.54) in NC-2. This data also suggested that Ag atoms in NC-2 were chemically bonded with Au atoms, also supported the location of Ag atoms in the M_{13} core;[31, 82] (2) The maximum number of Ag atoms that can be doped in Au_{25} NCs was below 13 regardless of the addition of excess Ag precursors. For example, Figure 2.8 showed that either $(AuAg)_{25}$ NCs with a doped Ag atom number below 13 or

no $(AuAg)_{25}$ NCs have been formed when further increasing the feed ratios $R_{Au/Ag}$ to 12/13 or 5/20; (3) Since the as-synthesized $(AuAg)_{25}MHA_{18}$ NCs have the same number of metal atoms (25) and ligands (18) as the thiolated Au_{25} NCs, a geometric similarity of $(AuAg)_{25}$ NCs and Au_{25} NCs should be favorably preserved. In addition, recent studies have resolved the motif structures of thiolated Ag NCs, which are Ag_2-SR_5, distinctively different from the motifs in thiolated Au NCs, such as Au_2-SR_3.[40, 127] This data also suggests that Ag atoms were most likely incorporated in the M_{13} core, and did not involve in the formation of Ag-thiolate motifs in the outer M_{12} shell.

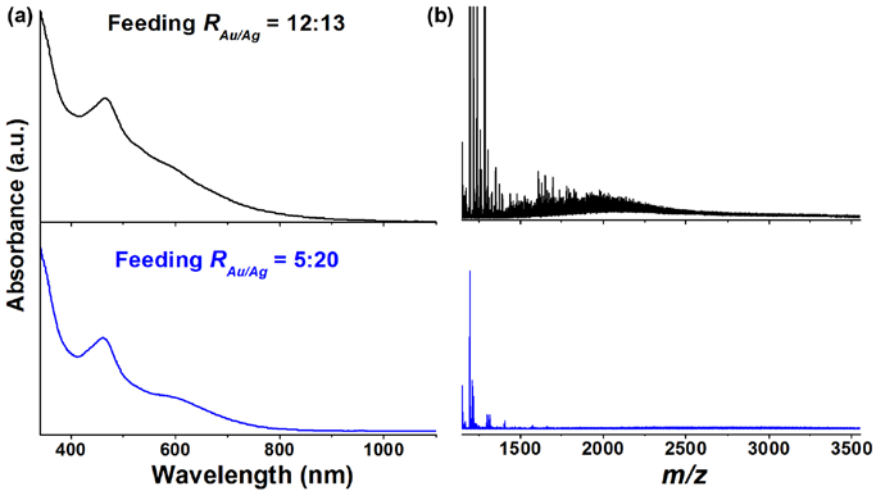

Figure 2.8 (a) UV-vis absorption and (b) ESI mass spectra of the MHA-protected AuAg NCs synthesized at feeding ratio $R_{Au/Ag}$ of 12/13 (upper panel, black lines), and 5/20 (lower panel, blue lines).

Our synthetic protocol is fairly generic and can be easily adopted to synthesize $(AuAg)_{25}$ NCs protected by other hydrophilic thiolate ligands. For example, two relatively larger thiolate ligand, C_8-chain 8-mercaptooctanoic acid (MOA) and C_{11}-chain 11-mercaptoundecanoic acid (MUA), can be chosen as protecting ligands. As shown in Figure 2.9a and 2.10a, the as-synthesized MOA- and MUA-protected (AuAg) NCs showed the identical absorptions as that of MHA-protected $(AuAg)_{25}$ NCs (Figure 2.2b). ESI mass

spectra of MOA-protected AuAg NCs (Figure 2.9b) suggest their formulas to be $Au_{23-25}Ag_{2-0}(MOA)_{18}$, $Au_{20-23}Ag_{5-2}(MOA)_{18}$, and $Au_{15-19}Ag_{10-6}(MOA)_{18}$ when the feeding ratios of $R_{Au/Ag}$ of 24:1, 14:11, and 12:13 (Figure 2.9c), respectively. Similarly, the formulas of MUA-protected AuAg NCs determined by their ESI mass spectra (Figure 2.10b) were $Au_{23-25}Ag_{2-0}(MUA)_{18}$, $Au_{19-23}Ag_{6-2}(MUA)_{18}$, and $Au_{16-22}Ag_{9-3}(MUA)_{18}$ when the feeding ratios of $R_{Au/Ag}$ of 24/1, 16/9, and 14/11(Figure 2.10c), respectively. It should be noted that the synthesis of various thiolate ligands-protected NCs realized by this method could provide a platform for ligand-related fundamental studies (e.g., ligand effects on NCs' stability, and the performances of interface-involved applications). In principle, our synthetic protocol could also be extended to synthesize AuAg NCs protected by other thiolate ligands (e.g., cysteine, glutathione, and etc.) and bimetallic NCs with other metal ingredients (e.g. AuPd and AuCu).

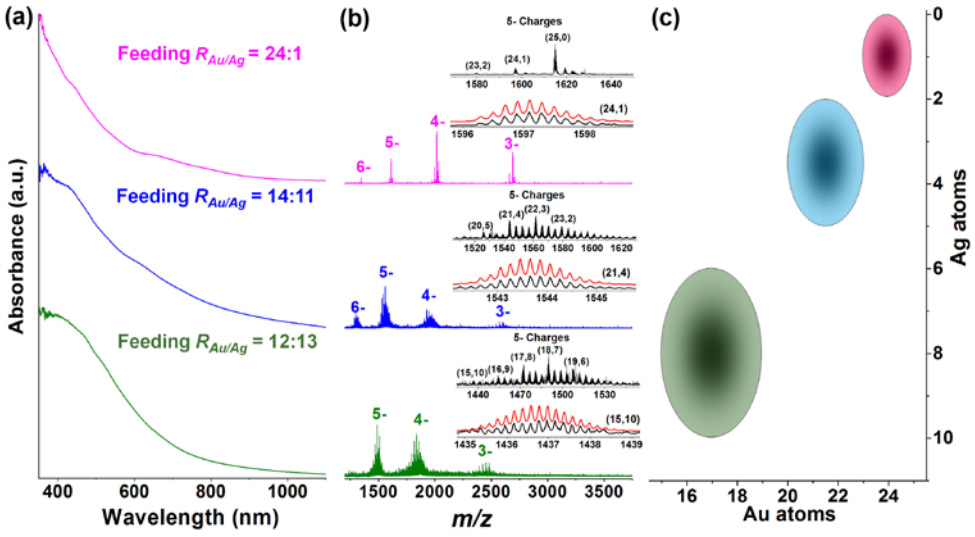

Figure 2.9 (a) UV-vis absorption spectra, (b) ESI mass spectra, and compositional distributions of MOA-protected $(AuAg)_{25}$ NCs prepared at feeding $R_{Au/Ag}$ of 24/1 (pink), 14/11 (blue), and 12/13 (green). Insets in Figure 2.9b are zoom-in ESI spectra of 5- charged species of the as-synthesized AuAg NCs (upper panel) and representative isotope patterns (lower panel) derived theoretically (red) and experimentally (black). Figure 2.9c indicates

that the as-synthesized MOA-protected $(AuAg)_{25}$ NCs have different metal compositions: $Au_{23\text{-}25}Ag_{2\text{-}0}$ ($R_{Au/Ag}$=24/1); $Au_{20\text{-}23}Ag_{5\text{-}2}$ ($R_{Au/Ag}$=14/11), and $Au_{15\text{-}19}Ag_{10\text{-}6}$($R_{Au/Ag}$ = 12/13).

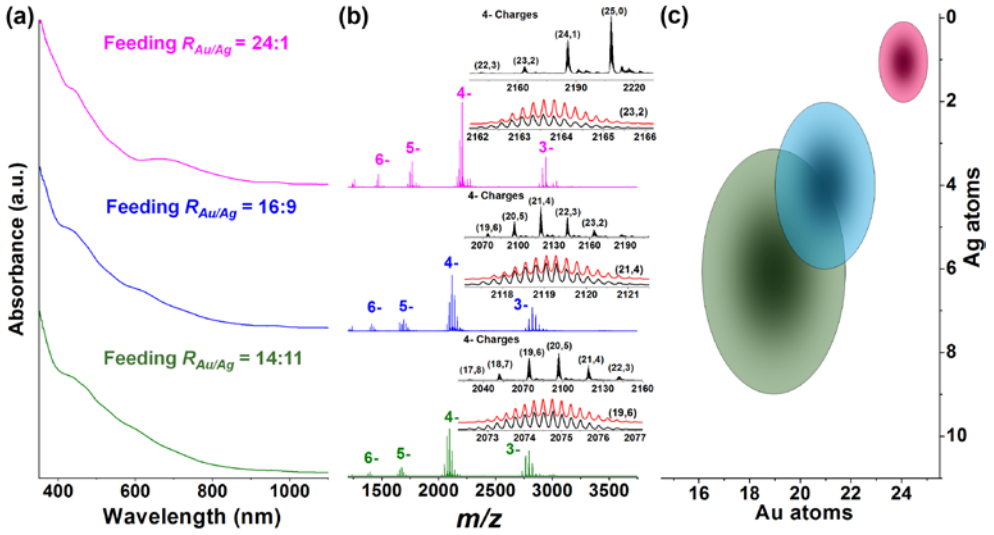

Figure 2.10 (a) UV-vis absorption spectra, (b) ESI mass spectra, and compositional distributions of MUA-protected $(AuAg)_{25}$ NCs prepared at feeding ratio of $R_{Au/Ag}$ of 24/1 (pink), 16/9 (blue), and 14/11 (green). Insets in Figure 2.10b are zoom-in ESI spectra of 4- charged species of the as-synthesized AuAg NCs (upper panel) and representative isotope patterns (lower panel) acquired theoretically (red) and experimentally (black). Figure 2.10c indicates that the as-synthesized MUA-protected $(AuAg)_{25}$ NCs have different metal composition: $Au_{23\text{-}25}Ag_{2\text{-}0}$ ($R_{Au/Ag}$ = 24:1), $Au_{19\text{-}23}Ag_{6\text{-}2}$ ($R_{Au/Ag}$ =16:9), $Au_{16\text{-}22}Ag_{9\text{-}3}$($R_{Au/Ag}$ =14:11).

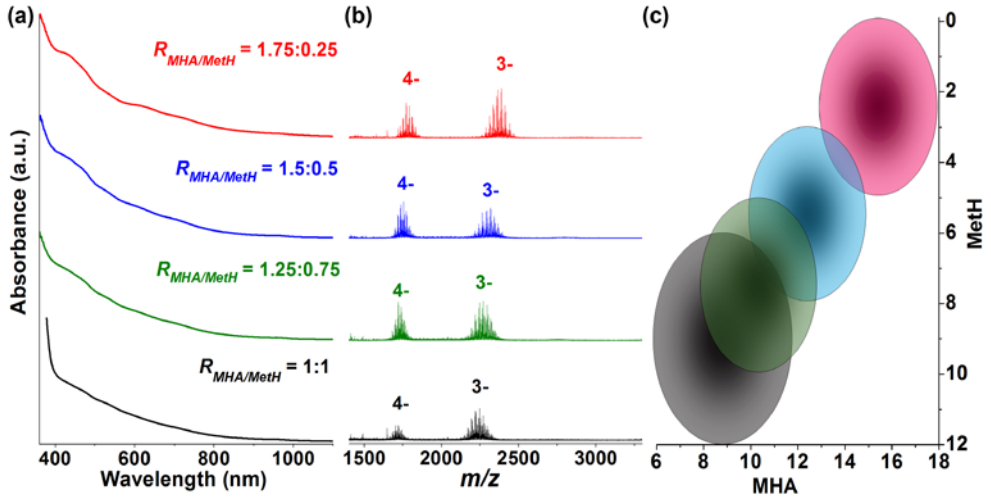

Figure 2.11 (a) UV-vis absorption, (b) ESI mass spectra (in negative ion mode), and (c) hetero-ligand distributions of the as-synthesized bi-thiolate-protected $(AuAg)_{25}(MHA/MetH)_{18}$ NCs with the same feeding ratio of $R_{Au/Ag}$ 22/3, but different feeding ratios of $R_{MHA/MetH:}$ 1.75:0.25 (red), 1.5:0.5 (blue), 1.25:0.75 (green), and 1:1 (black).

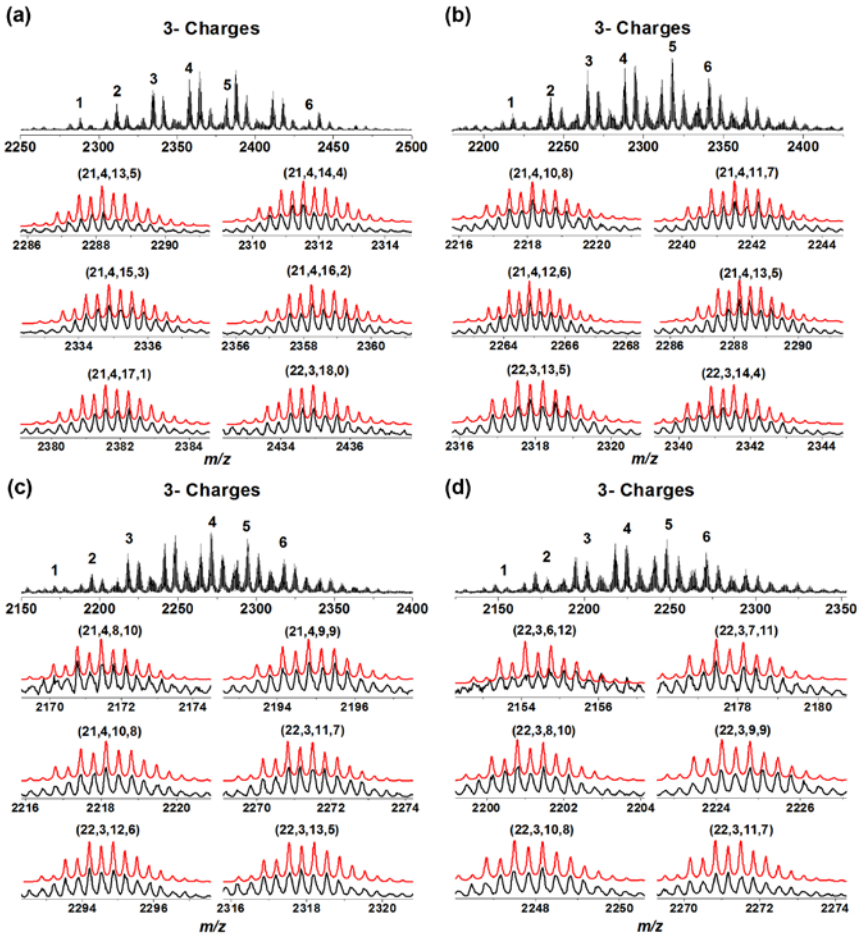

Figure 2.12 Zoom-in ESI mass spectra and representative isotope patterns (theoretical / red, and experimental / black) of 3- charged MHA/MetH-protected $(AuAg)_{25}$ NCs prepared by keeping the feeding ratio $R_{Au/Ag}$ of 22/3, but varying the feeding ratio $R_{MHA/MetH}$ from 1.75/0.25 (a), 1.5/0.5 (b), 1.25/0.75 (c), to 1/1 (d). The numbers within the bracket are the number of Au atoms, Ag atoms, MHA, and MetH in $(AuAg)_{25}(MHA/MetH)_{18}$ NCs. For example, (21, 4, 13, 5) is denoted as $Au_{21}Ag_4(MHA_{13}MetH_5)$ NC species.

Another salient advantage of our synthetic protocol is to make the synthesis of $(AuAg)_{25}$ NCs with controlled ligand combinations possible, generating AuAg NCs with tailorable ligand surface. As a simple demonstration, we rationally introduced the hydroxyl groups to the AuAg NC surface by using a thiol-containing alkanoic alcohol [e.g., 2-mercaptoethanol (MetH)] in combination with the thiol-containing alkanoic acid (e.g., MHA) as protecting ligands during the synthesis of $(AuAg)_{25}$ NCs. As shown in Figure 2.11, by adjusting the feeding ratios of $R_{MHA/MetH}$ from 1.75/0.25, 1.5/0.5,

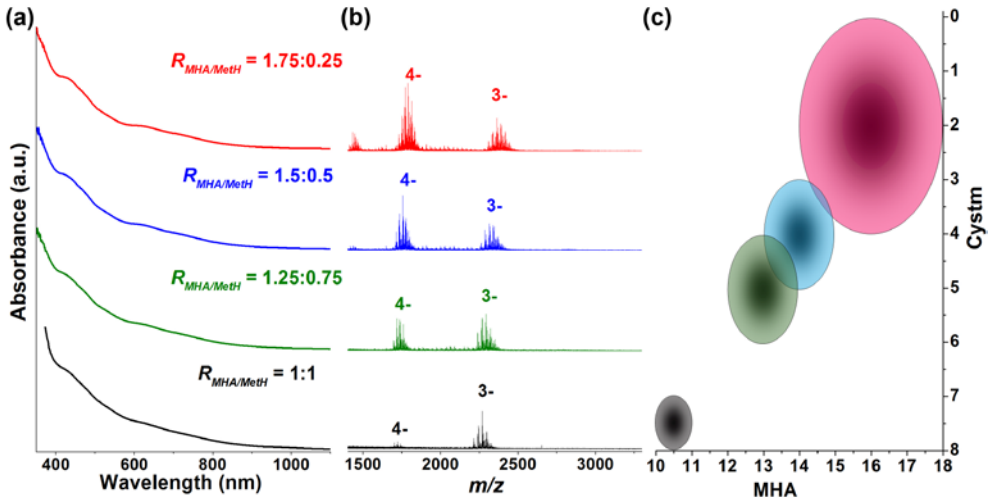

Figure 2.13 (a) UV-vis absorption, (b) ESI mass spectra (in negative ion mode), and (c) hetero-ligand distributions of MHA/Cystm-protected $(AuAg)_{25}$ NCs synthesized by keeping feeding ratio $R_{Au/Ag}$ of 22:3, but varying feeding ratio $R_{MHA/Cystm}$ from 1.75/0.25 (red), 1.5/0.5 (blue), and 1.25/0.75 (green), to 1/1 (black). Figure 2.13c indicates that the as-synthesized MHA/Cystm-protected $(AuAg)_{25}$ NCs have different hetero-ligand distributions: $MHA_{14-18}Cystm_{4-0}$ ($R_{MHA/Cystm}$=1.75/0.25), $MHA_{13-15}Cystm_{5-3}$ ($R_{MHA/Cystm}$=1.5/0.5), $MHA_{12-14}Cystm_{6-4}$ ($R_{MHA/Cystm}$=1.25/0.75), and $MHA_{10-11}Cystm_{8-7}$ ($R_{MHA/Cystm}$ = 1/1).

1.25/0.75, to 1/1, while keeping the other reaction conditions the same (the feeding ratio of $R_{Au/Ag}$ was 22/3), we can obtained MHA/MetH-protected AuAg NCs, which showed identical UV-vis absorption features (Figure 2.11a) as that of MHA-protected $(AuAg)_{25}$ NCs (Figure 2.2a). ESI mass spectra suggest that the as-synthesized MHA/MetH-protected AuAg NCs (Figure 2.11b) were $(AuAg)_{25}(MHA)_{13-18}(MetH)_{5-0}$, $(AuAg)_{25}(MHA)_{10-15}(MetH)_{8-3}$, $(AuAg)_{25}(MHA)_{8-13}(MetH)_{10-5}$, and $(AuAg)_{25}(MHA)_{6-12}(MetH)_{12-6}$ NCs, which were also illustrated in Figure 2.11c. Their zoom-in ESI mass spectra as well as the representative isotope patterns were presented in Figure 2.12. It should be noted that the incorporation of Ag atoms in AuAg NCs could partially widen the hetero-ligand distributions compared to that in Au NC system. Furthermore, other functional groups (e.g., amine) can also be easily tethered to the AuAg NC surface. For example, by using cysteamine (Cystm)

with MHA as protecting ligands, and varying their feeding ratios ($R_{MHA/Cystm}$ from 1.75/0.25, 1.5/0.5, 1.25/0.75, to 0.75/1.25, a series of MHA/Cystm-protected $(AuAg)_{25}$ NCs with well-controlled hetero-ligand distributions were obtained (Figure 2.13-2.14).

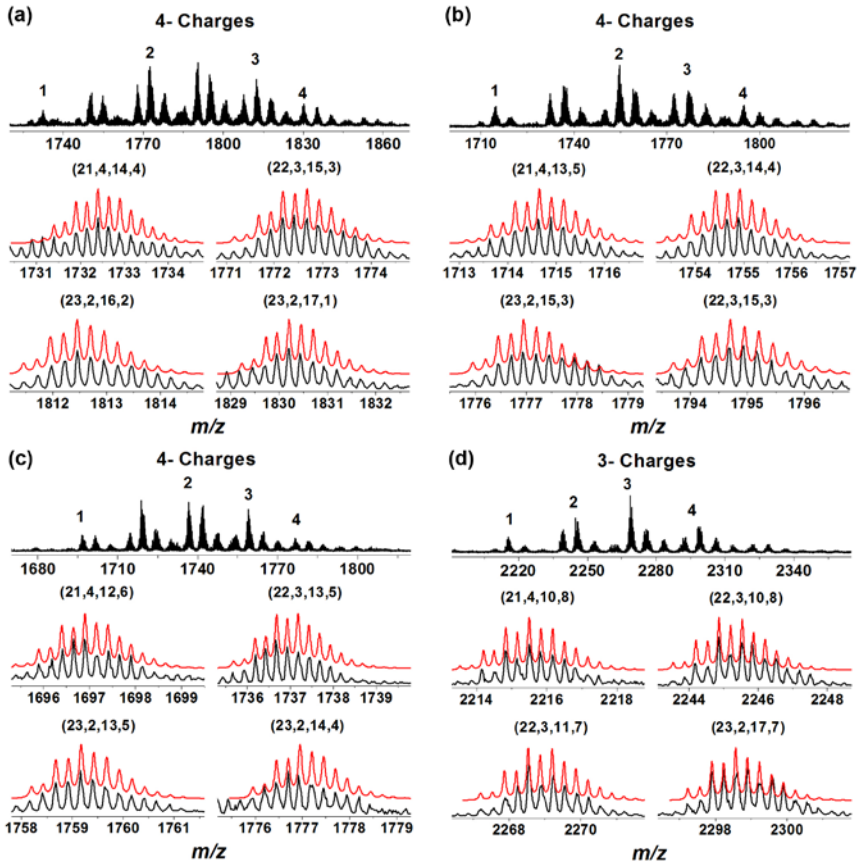

Figure 2.14 Zoom-in ESI mass spectra and representative isotope patterns (theoretical / red, and experimental / black) of 4- or 3- charged MHA/Cystm-protected $(AuAg)_{25}$ NCs prepared by keeping the feeding ratio $R_{Au/Ag}$ of 22/3, but varying the feeding ratio $R_{MHA/MetH}$ from 1.75/0.25 (a), 1.5/0.5 (b), 1.25/0.75 (c), to 1.0/1.0 (d). The numbers within the bracket are the number of Au atoms, Ag atoms, MHA, and Cystm in $(AuAg)_{25}(MHA/Cystm)_{18}$ NCs. For example, (21, 4, 14, 4) is denoted as $Au_{21}Ag_4(MHA_{14}MetH_4)$ NC species.

2.4 Conclusion

In this chapter, we have developed a facile and efficient method to synthesize a series of water-soluble $(AuAg)_{25}$ NCs protected by mono- and bi-thiolate ligands via the NaOH-mediated $NaBH_4$-reduction method. The key of

our protocol was to use the different interactions between thiolate-Au and thiolate-Ag to minimize their different redox potentials, making the formation of alloyed AuAg NCs possible. The compositions of both the metal core and ligand shell can be continuously tailored by varying the feeding ratios of metal precursors ($R_{Au/Ag}$) and hetero-ligands ($R_{MHA/MetH}$ and $R_{MHA/Cystm}$), greatly enriching the combinational functionalities of the NCs. The synthetic method and products developed in this study are of interest in the cluster community not only because they have enriched the library of NC family to further advance their practical applications, but also because this study sheds some light on the design of new synthetic strategies efficient enough for the synthesis of bi-metallic NCs with multi-functionalities.

CHAPTER 3 LIGHTING UP THIOLATED Au@Ag NANOCLUSTERS VIA AGGREGATION-INDUCED EMISSION

3.1 Introduction

Thiolate-protected gold and silver nanoclusters or thiolated Au/Ag NCs, are ultrasmall NPs containing up to several hundred Au/Ag atoms, which are stabilized by a certain number of thiolate ligands in solution.[1, 6] Owing to the strong quantum confinement effects in this sub-2 nm size regime, thiolated Au/Ag NCs have discrete and size-dependent electronic structures[128] and therefore show unique molecular-like properties such as quantized charging,[12, 129] magnetism,[7, 8] and strong luminescence.[4, 16, 130, 131] These properties are, however, not observed in their larger counterparts, which are relatively large Au/Ag NPs with core sizes above 2 nm.[38, 132, 133] The strong luminescence of thiolated Au/Ag NCs is one crucial feature for many of their practical applications. For example, luminescent Au/Ag NCs have recently emerged as a new type of promising luminescent probes for a variety of biomedical applications including bioimaging and biosensing.[3, 5, 20, 27, 119, 134, 135] These applications have also attracted rapidly growing interests from the research community in developing efficient synthesis strategies for highly luminescent Au/Ag NCs.[2, 4, 46]

Very recently, we reported a new type of highly luminescent thiolated Au NCs with a core-shell Au(0)@Au(I)-thiolate nanostructure.[14] Such Au NCs showed very strong luminescence in aqueous solution, and their luminescence

was generated from the large Au(I)-thiolate complexes on the NC surface via aggregation-induced emission (AIE). We have successfully produced this AIE-type luminescent Au NCs with a high quantum yield (QY) of ~15%. However, it is still unclear whether the AIE could also be used to synthesize other luminescent MNCs such as Ag and bimetallic NCs, which is the aim of our current investigation. In this chapter, we report a novel and facile synthesis strategy for highly luminescent bimetallic AuAg NCs that can show luminescence via AIE. To the best of our knowledge, this is the first demonstration of an AIE-type luminescent AuAg NCs.

Our target materials are bimetallic AuAg NCs,[31, 35, 82] which are expected to have synergistic effects in their physicochemical properties compared with their mono-metallic analogues.[39, 42, 136, 137] There are three major synthesis approaches for bimetallic AuAg NCs in the current development. The first approach is co-reduction (a typical one-pot synthesis method), where Au and Ag precursors (e.g., $HAuCl_4$ and $AgNO_3$) are first mixed, followed by the introduction of a particular reducing agent, leading to the formation of bimetallic AuAg NCs.[31, 33, 79] The second approach is galvanic replacement (a typical two-pot synthesis method), where Ag NCs were first prepared, followed by the addition of Au(III) ions to oxidize the Ag NCs on the basis of the galvanic replacement reaction, resulting in the formation of bimetallic AuAg NCs.[35] The third approach is anti-galvanic replacement, where Au NCs were first prepared, followed by the introduction of Ag(I) ions to replace Au atoms in the Au NCs, leading to the formation of bimetallic AuAg NCs.[50] These three approaches are efficient for the synthesis of bimetallic AuAg NCs; however, they often produce AuAg NCs with weak luminescence. To address

this issue, in this chapter, we present a new approach to synthesize highly luminescent bimetallic Au@Ag NCs, where a particular weakly luminescent thiolated Au NC species (hereafter referred to as parental Au NCs) was first prepared, followed by the introduction of Ag(I) ions. Interestingly, after ~15 min, an unexpected strong luminescence was observed from the as-synthesized Au@Ag NCs. The luminescence light-up process is illustrated in Figure 3.1a, where, upon addition, the Ag(I) ions immediately link the small Au(I)-thiolate motifs on the parental NC surface, forming a grid network or large Au(I)/Ag(I)-thiolate motifs around the entire NC surface, which can light up the thiolated AuAg NCs via AIE.

3.2 Experimental Section

3.2.1 Materials

All chemicals were used as received: hydrogen tetrachloroaurate(III) trihydrate ($HAuCl_4 \cdot 3H_2O$) from Alfa Aesar; silver nitrate ($AgNO_3$) and sodium hydroxide (NaOH) from Merck; L-cysteine (Cys), L-glutathione reduced (GSH), 2,5-dihydroxybenzoic acid (DHB) from Sigma-Aldrich. Ultrapure Millipore water (18.2 MΩ) was used throughout the study. All glassware and poly-tetrafluoroethylene-coated magnetic stir bars were cleaned with *aqua regia* and rinsed with copious water and ethanol before drying in the oven.

3.2.2 Characterization

UV-vis absorption and luminescence spectra were recorded on a Shimadzu UV-1800 spectrometer and a PerkinElmer LS55 fluorescence spectrometer, respectively. Luminescence lifetimes were analyzed by the time-

correlated single-photon counting (TCSPC) on a Horiba Jobin Yvon Fluorolog-3 spectrofluorometer. X-ray photoelectron spectroscopy (XPS) was performed on a Kratos AXIS Ultra^{DLD} spectrometer (Kratos Analytical Ltd). Transmission electron microscopy (TEM) was carried out on a JEOL JEM 2010 microscope operating at 200 kV. The size of the NCs was measured by matrix-assisted laser desorption ionization-time-of-flight (MALDI-TOF) mass spectrometry on a Bruker Daltonics Autoflex II TOF/TOF system. Saturated DHB solution was selected as the matrix for MALDI-TOF measurements. Dialysis tubing of 3000 Da molecular weight cut off (MWCO) was used for the purification of the NCs. The composition of the NCs was analyzed by inductively coupled plasma - mass spectroscopy (ICP-MS) on an Agilent 7500A. Native polyacrylamide gel electrophoresis (PAGE) was carried out on a Bio-Rad Mini-Protean Tetra Cell system. 30 and 4 wt% acrylamide monomers were prepared for resolving and stacking gels, respectively. Sample solutions were loaded in the stacking gel. The electrophoresis was allowed to run at 4 °C with a constant voltage of 170 V.

3.2.3 Synthesis of Highly Luminescent GSH-Protected Au@Ag NCs

The parental GSH-protected Au NCs [i.e., $Au_{18}(SG)_{14}$, $Au_{15}(SG)_{13}$, and $Au_{25}(SG)_{18}$] were prepared by a reported carbon monoxide (CO)-reduction method.[60,54] The as-prepared Au NCs were then purified by dialysis for about 9 h. To synthesize Au@Ag NCs, an aqueous $AgNO_3$ solution (0.5 mL, 2 mM) was introduced to the purified parental Au_{18} NCs (5 mL, 0.8 mM) under a vigorous stirring condition (1000 rpm). The reaction was allowed to proceed for ~15 min, and the as-synthesized Au_{18}@Ag NCs were collected for further characterizations.

3.3 Results and Discussion

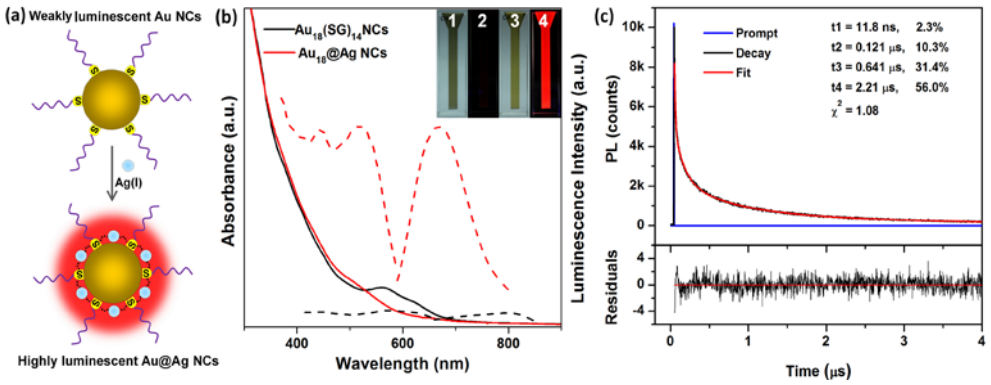

Figure 3.1 (a) Schematic illustration of the light-up process for the synthesis of highly luminescent Au@Ag NCs by using Ag(I) ions as linkers in connecting the small Au(I)-thiolate motifs on the parental Au NC surface. (b) UV-vis absorption (solid lines) and photoemission (dashed lines, λ_{ex} = 520 nm) spectra of the parental $Au_{18}(SG)_{14}$ NCs (black lines) and luminescent Au@Ag NCs (red lines). (Insets) Digital photos of the parental $Au_{18}(SG)_{14}$ NCs (item 1 and 2) and luminescent Au@Ag NCs (item 3 and 4), under visible (item 1 and 3) and UV (item 2 and 4) light. (c) Luminescence decay profiles (top panel) of the luminescent Au@Ag NCs. The red line is a tetra-exponential fit of the experimental data. The bottom panel shows the residuals of fitting.

We showed this concept by using a well-studied glutathione (GSH)-protected Au NCs[62, 138] as the parental Au NCs. GSH is a natural tripeptide containing one thiol group in its Cys residue. The GSH-protected Au NCs were prepared according to a reported carbon monoxide (CO)-reduction method.[54, 60] As a proof-of-concept, $Au_{18}(SG)_{14}$ was chosen as a model of parental Au NC in this study. The as-prepared parental $Au_{18}(SG)_{14}$ NCs were greenish-brown in aqueous solution (Figure 3.1b, inset, item 1). No visible luminescence was observed in the NC solution under UV illumination at 365 nm (Figure 3.1b, inset, item 2). The weak luminescence of $Au_{18}(SG)_{14}$ was located at~800 nm (Figure 3.1b, dashed black line), with a low QY of 0.37 if rhodamine B was used as reference, which is similar so the observation in previous report.[62] The parental Au NCs also featured two distinct absorption peaks at 560 and 620 nm in the UV-vis region (Figure 3.1b, solid black line),

which are the absorption characteristics of $Au_{18}(SG)_{14}$ NCs.[54] The well-defined absorption spectrum also suggests high-purity $Au_{18}(SG)_{14}$ NCs in the as-prepared parental Au NCs.

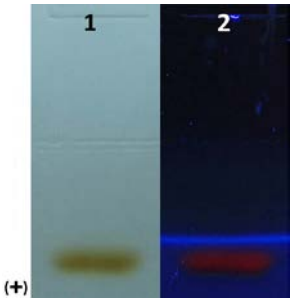

Figure 3.2 Digital photos of the PAGE gel of the as-synthesized luminescent Au_{18}@Ag NCs under visible (lane 1) and UV (lane 2) light.

After the introduction of a certain amount of Ag(I) ions, the initially greenish-brown $Au_{18}(SG)_{14}$ NCs (Figure 3.1b, inset, item 1) was instantaneously changed to brown (inset, item 3) in aqueous solution. Accordingly, the characteristic absorption peaks of the parental $Au_{18}(SG)_{14}$ NCs (560 and 620 nm) disappeared, and a new shoulder peak at ~520 nm appeared in the reaction solution (Figure 3.1b, red solid line). More interestingly, strong red emission was observed in the reaction solution at ~15 min (Figure 3.1b, inset, item 4), which is in stark contrast to the weak luminescence of the parental $Au_{18}(SG)_{14}$ NCs (inset, item 2). The emission peak of the as-synthesized Au@Ag NCs was located at 667 nm (Figure 3.1b, dashed red line). The QY was ~6.8% using rhodamine B as a reference. The excitation spectrum (dashed red line, Figure 3.1b) of the as-synthesized Au@Ag NCs also matches nicely with its UV-vis absorption spectrum (solid red line, Figure 3.1b). Moreover, only one distinct band was observed in the native polyacrylamide gel electrophoresis (PAGE, 30%) of the as-synthesized Au@Ag NCs (Figure 3.2, lane 1), and this band showed strong red emission

under UV illumination (lane 2). These data suggest that the strong luminescence observed in the reaction solution was emitted by the as-synthesized Au@Ag NCs, rather than from the impurities or side products in the reaction solution. TEM images also suggest the ultrasmall size feature (<2 nm) of the as-synthesized luminescent Au@Ag NCs (Figure 3.3b), which is similar to the size of the parental Au NCs (Figure 3.3a).

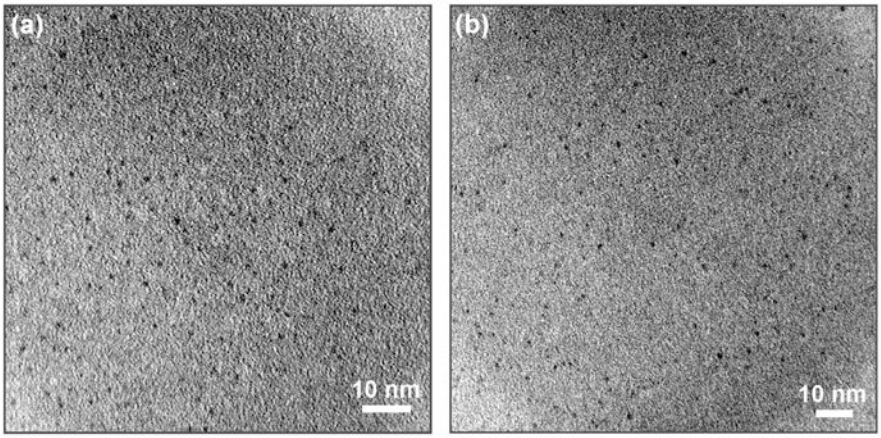

Figure 3.3 Representative TEM images of (a) the parental Au_{18} NCs and (b) the as-synthesized luminescent Au_{18}@Ag NCs.

The luminescence property of the as-synthesized Au@Ag NCs was further examined by luminescence lifetime measurements. As shown in Figure 3.1c, the luminescence decay response suggests the predominance of long lifetime (in the microsecond scale) components in the luminescent Au@Ag NCs: 2.21 μs (56%), 0.641 μs (31.4%), 0.121 μs (10.3%), and 11.8 ns (2.3%). The microsecond-scale lifetimes in the luminescent Au@Ag NCs were similar to the lifetimes of the previously reported AIE-type luminescent Au NCs.[14] These data suggest that the emission of the as-synthesized Au@Ag NCs was generated from the AIE of Au(I)/Ag(I)-thiolate complexes on the NC surface, which is phosphorescence via the metal-centered triplet states. This luminescence pathway is distinctly different from the nanosecond emission

from the singlet excited states of previously reported luminescent Ag NCs protected by DNA.[5]

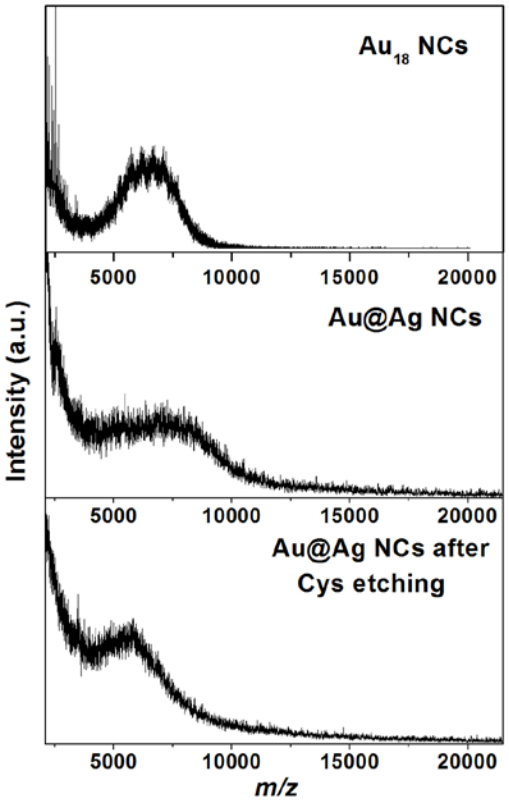

Figure 3.4 MALDI-TOF mass spectra of the parental Au_{18} NCs (top panel), as-synthesized luminescent Au_{18}@Ag NCs (middle panel), and luminescent Au_{18}@Ag NCs after the addition of a certain amount of Cys (bottom panel).

MALDI-TOF mass spectrometry was then used to examine the composition of the parental Au NCs and as-synthesized luminescent Au@Ag NCs. It should be noted that extensive fragmentations often occur in the MALDI-TOF measurements.[69, 139] As shown in Figure 3.4, a broad spectrum in the mass range of 5270 to 7840 Da was observed for the parental Au NCs (top panel), which could be assigned to $Au_{18}(SG)_{14}$ (the calculated molecular weight of 7834 Da) and its fragmentation to various extents. In contrast, the as-synthesized luminescent Au@Ag NCs showed a broader mass spectrum from 5270 to 8600 Da (Figure 3.4, middle panel), where a molecular weight increase of up to 760 Da (= 8600 - 7840) was seen when compared to the

parental Au NCs. This molecular weight difference is most likely contributed by the Ag atoms attached to the parental Au NCs. From the calculation, about one to seven Ag atoms are in the as-synthesized luminescent Au@Ag NCs.

The as-synthesized Au@Ag NCs showed strong luminescence via the AIE of the complexes on the NC surface, where the size/structure of the Au(I)/Ag(I)-thiolate complexes is the key in determining their strong luminescence in visible to near-infrared region. We hypothesized that the strong red emission in the as-synthesized Au@Ag NCs is generated by connecting the small Au(I)-thiolate motifs on the parental Au NCs via the Ag(I) linkers, forming large Au(I)/Ag(I)-thiolate motifs, which could generate strong luminescence via AIE. Since the Ag(I) ions serve as linkers in forming the large Au(I)/Ag(I)-thiolate complexes on the as-synthesized luminescent Au@Ag NCs, the removal of Ag(I) linkers may break those emission-active species [large Au(I)/Ag(I)-thiolate complexes] and scrub off those Ag(I) ions from the NC surface, which could revert the Au@Ag NCs back to the parental Au NCs, and as a result annul their strong luminescence in solution. The proposed luminescence quenching process is illustrated in Figure 3.5a. The Ag(I) linkers on the luminescent Au@Ag NCs are removed by the introduction of a particular thiolate ligand, such as Cys, which can interact strongly with Ag(I) ions via the formation of Ag(I)-thiolate complexes. As expected, the strong red emission of the as-synthesized Au@Ag NCs was immediately quenched upon the addition of Cys to the NC solution (Figure 3.5b, item 2). Accordingly, the emission peak of the as-synthesized Au@Ag NCs at 667 nm disappeared after the addition of a certain amount of Cys in the NC solution (Figure 3.5b, black line).

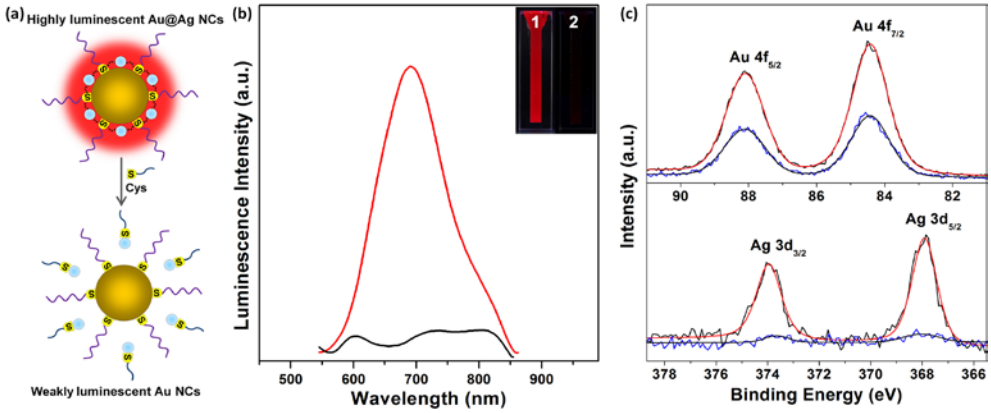

Figure 3.5 (a) Schematic illustration of the luminescence quenching of the as-synthesized luminescent Au@Ag NCs by using Cys to selectively remove the Ag(I) linkers from the Au@Ag NC surface, which breaks the large Au(I)/Ag(I)-thiolate motifs on the NC surface and thus annul their strong luminescence in solution. (b) Photoemission spectra (λ_{ex} = 520 nm) of the as-synthesized luminescent Au@Ag NCs (red line) and that after the introduction of Cys (black line). (Insets) Digital photos of the as-synthesized luminescent Au@Ag NCs (item 1) and that after the Cys was added (item 2) under UV illumination. (c) XPS spectra of the Au 4f (top panel) and Ag 3d (bottom panel) of the as-synthesized luminescent Au@Ag NCs (red lines) and that after the introduction of Cys (blue lines).

XPS and ICP-MS were also used to obtain the composition information of the Au@Ag NCs before and after the addition of Cys. The molar ratio of Au:Ag in the luminescent Au@Ag NCs was found to be 1:0.21 by XPS analysis (Figure 3.5c). This value was also confirmed by ICP-MS analysis with a typical value of 1:0.24. It should be mentioned that the composition data of the luminescent Au@Ag NCs are also consistent with the number of Ag atoms (1-7 Ag atoms per cluster) in the Au@Ag NCs estimated from their MALDI-TOF mass spectra (Figure 3.4). The Ag species in the luminescent Au@Ag NCs are Ag(I), which is confirmed by the XPS analysis of the binding energies of Ag $3d_{5/2}$ in the luminescent Au@Ag NCs. The binding energy of the Ag $3d_{5/2}$ in the luminescent Au@Ag NCs is 367.9 eV (Figure 3.5c, bottom panel, black line), which is identical to that of the Ag(I) species [Ag(I)-thiolate complexes as a control, Figure 3.6].[140] This is an expected result since the added Ag(I) ions only serve as linkers to bridge the small

Au(I)-thiolate motifs on the parental Au NC surface via the formation of strong Ag(I)-thiolate or metallophilic Ag(I)-Au(I) bond. In contrast, no obvious signal of Ag $3d_{5/2}$ was observed in the XPS spectrum of the luminescent Au@Ag NCs after the addition of Cys (Figure 3.5c, bottom panel, blue line). This information confirms the complete removal of Ag atoms from the luminescent Au@Ag NC surface by Cys. XPS and ICP-MS data provide further evidences on the complete removal of Ag atoms: the molar ratio of Au:Ag was 1:0.02 and 1:0.027, respectively. Taken together, these data strongly support that the strong red emission of the as-synthesized Au@Ag NCs was generated by connecting the small Au(I)-thiolate motifs on the parental Au NCs via the added Ag(I) linkers, leading to the formation of large Au(I)/Ag(I)-thiolate motifs and thus generating strong red emission via the AIE of such large motifs on the NC surface.

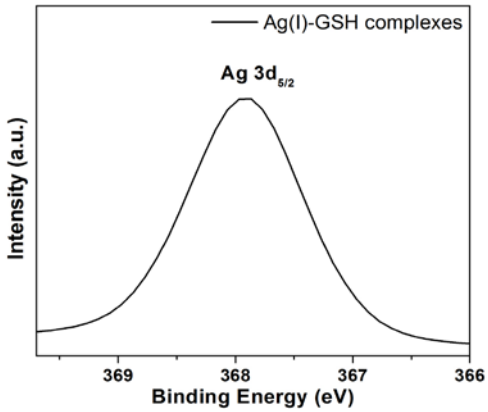

Figure 3.6 XPS spectrum of the Ag 3d species of the Ag(I)-GSH complexes.

The addition of Cys to the luminescent Au@Ag NCs removed the Ag(I) linkers from the large Au(I)/Ag(I)-thiolate motifs on the NC surface, and as a result the remnant NC species reverted back to thiolated Au NCs. This hypothesis was supported by XPS and MALDI-TOF analyses. It is well-documented that the oxidation states of MNCs are dictated by their size and structure. However, the binding energies of Au $4f_{7/2}$ in the luminescent

Au@Ag NCs before and after Ag(I) removal are identical at 84.4 eV (Figure 3.5c, top panel), implying that the removal of Ag(I) ions from the NC surface does not destruct the structure/size of the parental Au NCs and thus not affecting the oxidation states of Au in the NCs.[62] Furthermore, MALDI-TOF mass spectrum of the luminescent Au@Ag NCs after the removal of Ag(I) species from the NC surface showed a relatively narrow peak at ~5800 Da in the mass range of 2000 - 20000 Da (Figure 3.4, bottom panel), clearly revealing that Au NCs were preserved after the removal of the Ag(I) linkers despite its mass (~5800 Da) is smaller than that of the parental $Au_{18}(SG)_{14}$ NCs. The mass decrease of Au NCs after the addition of Cys could be understood from the possible removal of Au(I) from the NC surface considering that the affinity of Cys with Au(I) is also high.

Upscaling production of highly luminescent bimetallic Au@Ag NCs is another salient feature of the synthesis approach developed in this study (e.g., to 100 mL of luminescent Au@Ag NCs in a single batch, Figure 3.7a). In addition, our protocol is fairly generic and can be easily extended to synthesize other luminescent Au@Ag NCs by using different sized parental Au NCs. For example, if the non-luminescent $Au_{15}(SG)_{13}$ and $Au_{25}(SG)_{18}$ were used as the parental Au NCs (Figure 3.8), the as-synthesized Au_{15}@Ag NCs and Au_{25}@Ag NCs also showed very strong red emission under UV illumination (Figure 3.7b and 3.7c, inset, item 2). They also have similar photoemission spectra (Figure 3.7b and 3.7c) as that of luminescent Au@Ag NCs synthesized by using $Au_{18}(SG)_{14}$ as the parental Au NCs (Figure 3.1b, dashed red line). The emission peak of the as-synthesized luminescent

Au_{15}@Ag and Au_{25}@Ag NCs was located at 665 and 730 nm with a QY of 2.1% and 3.2%, respectively.

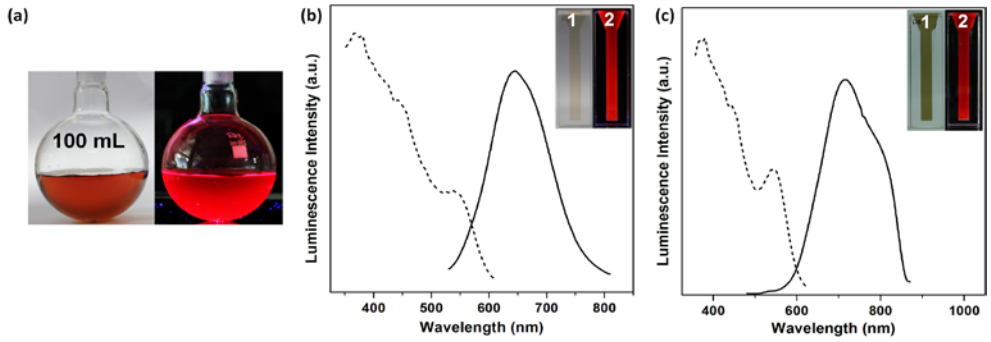

Figure 3.7 (a) Digital photos of the luminescent Au_{18}@Ag NCs synthesized in a 250 mL flask under visible (left) and UV (right) light. Photoemission (solid lines) and photoexcitation (dashed lines) spectra of the as-synthesized luminescent Au_{15}@Ag NCs (b) and Au_{25}@Ag NCs (c). (Insets) Digital photos of the as-synthesized luminescent Au@Ag NCs under visible (item 1) and UV (item 2) light.

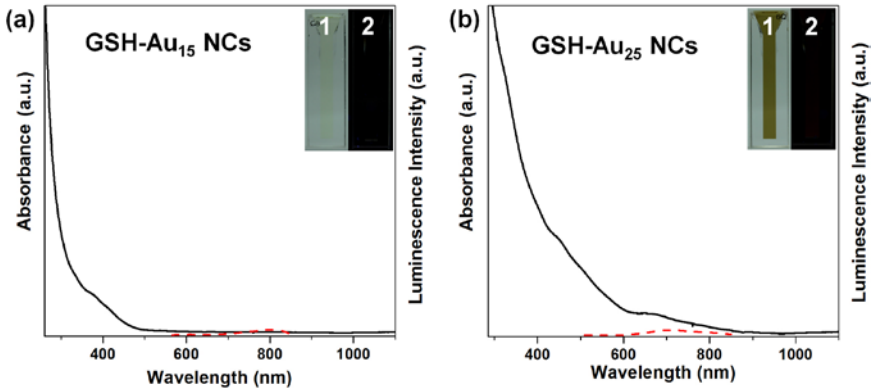

Figure 3.8 Optical absorption (solid lines), photoemission (dash lines) spectra, and digital photos (insets) of (a) the parental $Au_{15}(SG)_{13}$ NCs and (b) $Au_{25}(SG)_{18}$ NCs. Item 1 and 2 in the insets are taken under normal and UV light, respectively.

3.4 Conclusion

In this chapter, we have developed a new approach to synthesize highly luminescent Au@Ag NCs by using Ag(I) ions as linkers to bridge the small Au(I)-thiolate motifs on the weakly luminescent parental Au NCs, leading to the formation of large Au(I)/Ag(I)-thiolate motifs, which can generate strong luminescence via the AIE of the large complexes on the NC surface. The

protocols and products developed in this study are important not only because they provide a facile, fast (<15 min), scalable (≥100 mL), and generic approach for highly luminescent Au@Ag NCs, but more importantly because they exemplify that the AIE is a generalized principle in synthesizing luminescent thiolated noble MNCs.

CHAPTER 4

CONCLUSIONS AND RECOMMENDATIONS

4.1 Conclusions

Ultrasmall bi-MNCs have emerged as a new class of multi-functional NPs due to their ultrasmall size (typically below 2 nm), unique molecular-like properties (e.g., quantized charging and strong luminescence), controlled cluster compositions (at the atomic level), and synergistic physicochemical properties (integration of two metal species into one cluster). Currently, bi-MNCs have been mainly prepared through the one-step synthesis (i.e., co-reduction method), and the two-step approach relying on the different post-treatment including galvanic replacement, anti-galvanic replacement, and etching. Unfortunately, bi-MNCs prepared by the one-step approach are all hydrophobic and have poor surface functionalities, greatly restricting their biousabilities. On the other hand, most of bi-MNCs produced by the two-step approach possess non- or weak luminescence, and the underlying luminescence mechanism is unclear, which may limit the further advances of bi-MNCs as luminescent probes in biomedical applications. In this thesis, we aimed to 1) develop facile and general synthetic methods for the synthesis of water-soluble and monodisperse/luminescent AuAg bi-MNCs with either tunable metallic compositions/surface functionalities, or strong luminescence; and 2) understand the underlying luminescence mechanism of the as-synthesized bi-MNCs.

Firstly, a series of water-soluble $(AuAg)_{25}$ bi-MNCs protected by mono- and bi-thiolate ligands have been synthesized via NaOH-mediated $NaBH_4$ reduction method. Owing to differentiated interactions between thiolate-Au and thiolate-Ag, the selection of thiolate ligands in this study successfully minimizes the difference of Au and Ag in their redox potentials, and made the formation of alloy NCs possible. One advantage of this method is that both compositions of metallic core and the surface properties of ligand shell can be tailored by varying the feeding ratios of metal precursors and hetero-ligands, greatly expanding the combinational functionalities of the bi-MNCs, and potentially enhancing the bio-usability of the bi-MNCs.

Secondly, a simple strategy was developed to synthesize highly luminescent thiolated Au@Ag bi-MNCs by using Ag(I) ions as linkers to bridge small Au(I)-thiolate motifs on the weakly luminescent thiolated Au NCs, leading to the formation of large Au(I)/Ag(I)-thiolate motifs on the NC surface, which can generate strong luminescence via aggregation-induced emission (AIE). The protocols and products developed are important not only because they provide a facile, fast (<15 min), scalable (≥100 mL), and generic approach for highly luminescent Au@Ag NCs, but more importantly because they exemplify that the AIE is a generalized principle in synthesizing luminescent thiolated noble metal NCs (i.e., luminescence mechanism).

The developed strategies including NaOH-mediated $NaBH_4$ reduction and Ag deposition methods in this thesis are efficient in synthesizing water-soluble AuAg bi-MNCs with desired functionalities such as good biocompatibility, optional metallic compositions, rich surface functionalities, and strong luminescence, which provide a perfect platform for biomedical applications.

In addition, the strategies we developed may shed some light on the further design of new synthetic protocols and the production of other bi-MNCs.

4.2 Recommendations

Based on the preliminary results obtained in this thesis, several future works are recommended to further optimize the synthetic strategies, and exploit potential bioapplications of bi-MNCs.

Firstly, the application explorations of the as-synthesized bi-MNCs are of significant interests in future studies by making use of the unique features of the bi-MNCs such as ultrasmall size, good biocompatibility, excellent photo/thermo stabilities, optional metallic compositions, rich surface functionalities, and strong luminescence, which may help address some key issues related to the current sustainable development. For example, the Ag-based bi-MNCs could be a potent antimicrobial agent, especially to eradicate those multi-drug-resistant bacteria. Other promising applications of luminescent bi-MNCs are the design and development of theranostic probes for biomedical applications, such as drug delivery, and cancer diagnosis and treatment. For example, recently, Au NCs have been demonstrated to be a promising radiosensitizer for cancer radiotherapy. The multifunctional Au-Ag NCs may also do the same with an even better performance. The applications of bi-MNCs in other fields have begun to surface to the community, including in the fields of energy conversion (e.g., solar cell), environmental protection and monitor (e.g., toxic metal ion detection and remediation), and food safety; just name a few. Detailed and systemic investigations in these applications

could improve the performance of bi-MNCs and also to understand the working mechanisms of bi-MNCs in such applications.

Secondly, while the developed methods are efficient in synthesizing water-soluble bi-MNCs with quantities large enough for application explorations, more research efforts are expected to further tune synthetic conditions or modify the current methods for the synthesis of bi-MNCs with better qualities. In particular, the precise composition control of the bi-MNCs (or the ratio of two metals in one cluster) requires further efforts. The synthesis of bi-MNCs with anatomically precise composition may also facilitate some fundamental understandings of bi-MNCs, such as the correlation between the compositions and electronic structures, the effects of the compositions on the applications, and the influence of compositions (or continuous doping of a particular metal) on the cluster structures (e.g., the structural distortion). In addition, the as-synthesized bi-MNCs showed a relatively weak luminescence with a typical QY <10%, which may limit their use as luminescent probes for sensing and bioimaging applications, especially those applied in the in vivo settings.

References

[1] Jin, R. *Nanoscale* **2010**, *2*, 343-362.

[2] Yu, Y.; Yao, Q.; Luo, Z.; Yuan, X.; Lee, J. Y.; Xie, J. *Nanoscale* **2013**, *5*, 4606-4620.

[3] Shang, L.; Dong, S.; Nienhaus, G. U. *Nano Today* **2011**, *6*, 401-418.

[4] Diez, I.; Ras, R. H. A. *Nanoscale* **2011**, *3*, 1963-1970.

[5] Choi, S.; Dickson, R. M.; Yu, J. *Chem. Soc. Rev.* **2012**, *41*, 1867-1891.

[6] Lu, Y.; Chen, W. *Chem. Soc. Rev.* **2012**, *41*, 3594-3623.

[7] Negishi, Y.; Tsunoyama, H.; Suzuki, M.; Kawamura, N.; Matsushita, M. M.; Maruyama, K.; Sugawara, T.; Yokoyama, T.; Tsukuda, T. *J. Am. Chem. Soc.* **2006**, *128*, 12034-12035.

[8] Zhu, M.; Aikens, C. M.; Hendrich, M. P.; Gupta, R.; Qian, H.; Schatz, G. C.; Jin, R. *J. Am. Chem. Soc.* **2009**, *131*, 2490-2492.

[9] Li, Y.; Galli, G.; Gygi, F. o. *ACS Nano* **2008**, *2*, 1896-1902.

[10] Murray, R. W. *Chem. Rev.* **2008**, *108*, 2688-2720.

[11] Zhu, M.; Aikens, C. M.; Hollander, F. J.; Schatz, G. C.; Jin, R. *J. Am. Chem. Soc.* **2008**, *130*, 5883-5885.

[12] Chen, S.; Ingram, R. S.; Hostetler, M. J.; Pietron, J. J.; Murray, R. W.; Schaaff, T. G.; Khoury, J. T.; Alvarez, M. M.; Whetten, R. L. *Science* **1998**, *280*, 2098-2101.

[13] Yuan, X.; Yao, Q.; Yu, Y.; Luo, Z.; Dou, X.; Xie, J. *J. Phys. Chem. Lett.* **2013**, *4*, 1811-1815.

[14] Luo, Z.; Yuan, X.; Yu, Y.; Zhang, Q.; Leong, D. T.; Lee, J. Y.; Xie, J. *J. Am. Chem. Soc.* **2012**, *134*, 16662-16670.

[15] Yuan, X.; Luo, Z.; Zhang, Q.; Zhang, X.; Zheng, Y.; Lee, J. Y.; Xie, J. *ACS Nano* **2011**, *5*, 8800-8808.

[16] Zheng, J.; Zhou, C.; Yu, M.; Liu, J. *Nanoscale* **2012**, *4*, 4073-4083.

[17] Zhu, Y.; Qian, H.; Jin, R. *J. Mater. Chem.* **2011**, *21*, 6793-6799.

[18] Chen, Y.-S.; Choi, H.; Kamat, P. V. *J. Am. Chem. Soc.* **2013**, *135*, 8822-8825.

[19] Luo, Z.; Zheng, K.; Xie, J. *Chem. Commun.* **2014**, *50*, 5143-5155.

[20] Yuan, X.; Luo, Z.; Yu, Y.; Yao, Q.; Xie, J. *Chem-Asian J.* **2013**, *8*, 858-871.

[21] Xie, J.; Zheng, Y.; Ying, J. Y. *Chem. Commun.* **2010**, *46*, 961-963.

[22] Yuan, X.; Yeow, T. J.; Zhang, Q.; Lee, J. Y.; Xie, J. *Nanoscale* **2012**, *4*, 1968-1971.

[23] Yuan, X.; Tay, Y.; Dou, X.; Luo, Z.; Leong, D. T.; Xie, J. *Anal. Chem.* **2013**, *85*, 1913-1919.

[24] Shiang, Y.-C.; Huang, C.-C.; Chen, W.-Y.; Chen, P.-C.; Chang, H.-T. *J. Mater. Chem.* **2012**, *22*, 12972-12982.

[25] Yuan, X.; Setyawati, M. I.; Leong, D. T.; Xie, J. *Nano Res.* **2014**, *7*, 301-307.

[26] Yuan, X.; Setyawati, M. I.; Tan, A. S.; Ong, C. N.; Leong, D. T.; Xie, J. *NPG Asia Mater.* **2013**, *5*, e39.

[27] Chevrier, D. M.; Chatt, A.; Zhang, P. *J. Nanophotonics* **2012**, *6*, 064504.

[28] Kuznetsov, A. S.; Tikhomirov, V. K.; Shestakov, M. V.; Moshchalkov, V. V. *Nanoscale* **2013**, *5*, 10065-10075.

[29] Le Guevel, X. *IEEE J. Sel. Top. Quant. Electron.* **2014**, *20*, 1-12.

[30] Fields-Zinna, C. A.; Crowe, M. C.; Dass, A.; Weaver, J. E. F.; Murray, R. W. *Langmuir* **2009**, *25*, 7704-7710.

[31] Negishi, Y.; Iwai, T.; Ide, M. *Chem. Commun.* **2010**, *46*, 4713-4715.

[32] Gottlieb, E.; Qian, H.; Jin, R. *Chem. Eur. J.* **2013**, *19*, 4238-4243.

[33] Kumara, C.; Dass, A. *Nanoscale* **2012**, *4*, 4084-4086.

[34] Dou, X.; Yuan, X.; Yu, Y.; Luo, Z.; Yao, Q.; Leong, D. T.; Xie, J. *Nanoscale* **2014**, *6*, 157-161.

[35] Udayabhaskararao, T.; Sun, Y.; Goswami, N.; Pal, S. K.; Balasubramanian, K.; Pradeep, T. *Angew. Chem. Int. Ed.* **2012**, *51*, 2155-2159.

[36] Wang, D.; Li, Y. *Adv. Mater.* **2011**, *23*, 1044-1060.

[37] Zhang, Q.; Xie, J.; Liang, J.; Lee, J. Y. *Adv. Funct. Mater.* **2009**, *19*, 1387-1398.

[38] Yang, J.; Ying, J. Y. *Nat. Mater.* **2009**, *8*, 683-689.

[39] Huang, J.; Zhu, Y.; Lin, M.; Wang, Q.; Zhao, L.; Yang, Y.; Yao, K. X.; Han, Y. *J. Am. Chem. Soc.* **2013**, *135*, 8552-8561.

[40] Yang, H.; Wang, Y.; Huang, H.; Gell, L.; Lehtovaara, L.; Malola, S.; Häkkinen, H.; Zheng, N. *Nat. Commun.* **2013**, *4*, 2422.

[41] Zhang, H.; Watanabe, T.; Okumura, M.; Haruta, M.; Toshima, N. *Nat. Mater.* **2012**, *11*, 49-52.

[42] Qian, H.; Jiang, D.-e.; Li, G.; Gayathri, C.; Das, A.; Gil, R. R.; Jin, R. *J. Am. Chem. Soc.* **2012**, *134*, 16159-16162.

[43] Le Guevel, X.; Trouillet, V.; Spies, C.; Li, K.; Laaksonen, T.; Auerbach, D.; Jung, G.; Schneider, M. *Nanoscale* **2012**, *4*, 7624-7631.

[44] Zhou, T.-y.; Lin, L.-p.; Rong, M.-c.; Jiang, Y.-q.; Chen, X. *Anal. Chem.* **2013**, *85*, 9839-9844.

[45] Udayabhaskararao, T.; Pradeep, T. *J. Phys. Chem. Lett.* **2013**, *4*, 1553-1564.

[46] Maity, P.; Xie, S.; Yamauchi, M.; Tsukuda, T. *Nanoscale* **2012**, *4*, 4027-4037.

[47] Xie, S.; Tsunoyama, H.; Kurashige, W.; Negishi, Y.; Tsukuda, T. *ACS Catal.* **2012**, *2*, 1519-1523.

[48] Mohanty, J. S.; Xavier, P. L.; Chaudhari, K.; Bootharaju, M. S.; Goswami, N.; Pal, S. K.; Pradeep, T. *Nanoscale* **2012**, *4*, 4255-4262.

[49] Liu, G.; Feng, D.-Q.; Zheng, W.; Chen, T.; Li, D. *Chem. Commun.* **2013**, *49*, 7941-7943.

[50] Wu, Z. *Angew. Chem. Int. Ed.* **2012**, *51*, 2934-2938.

[51] Huang, C.-C.; Liao, H.-Y.; Shiang, Y.-C.; Lin, Z.-H.; Yang, Z.; Chang, H.-T. *J. Mater. Chem.* **2009**, *19*, 755-759.

[52] Brust, M.; Walker, M.; Bethell, D.; Schiffrin, D. J.; Whyman, R. *J. Chem. Soc., Chem. Commun.* **1994**, 801-802.

[53] Yao, Q.; Yu, Y.; Yuan, X.; Yu, Y.; Xie, J.; Lee, J. Y. *Small* **2013**, *9*, 2696-2701.

[54] Yu, Y.; Chen, X.; Yao, Q.; Yu, Y.; Yan, N.; Xie, J. *Chem. Mater.* **2013**, *25*, 946-952.

[55] Wu, Z.; MacDonald, M. A.; Chen, J.; Zhang, P.; Jin, R. *J. Am. Chem. Soc.* **2011**, *133*, 9670-9673.

[56] Zhu, M.; Qian, H.; Jin, R. *J. Am. Chem. Soc.* **2009**, *131*, 7220-7221.

[57] Zhu, M.; Qian, H.; Jin, R. *J. Phys. Chem. Lett.* **2010**, *1*, 1003-1007.

[58] Heaven, M. W.; Dass, A.; White, P. S.; Holt, K. M.; Murray, R. W. *J. Am. Chem. Soc.* **2008**, *130*, 3754-3755.

[59] Yuan, X.; Yu, Y.; Yao, Q.; Zhang, Q.; Xie, J. *J. Phys. Chem. Lett.* **2012**, *3*, 2310-2314.

[60] Yu, Y.; Luo, Z.; Yu, Y.; Lee, J. Y.; Xie, J. *ACS Nano* **2012**, *6*, 7920-7927.

[61] Zeng, C.; Li, T.; Das, A.; Rosi, N. L.; Jin, R. *J. Am. Chem. Soc.* **2013**, *135*, 10011-10013.

[62] Negishi, Y.; Nobusada, K.; Tsukuda, T. *J. Am. Chem. Soc.* **2005**, *127*, 5261-5270.

[63] Zeng, C.; Qian, H.; Li, T.; Li, G.; Rosi, N. L.; Yoon, B.; Barnett, R. N.; Whetten, R. L.; Landman, U.; Jin, R. *Angew. Chem. Int. Ed.* **2012**, *51*, 13114-13118.

[64] Qian, H.; Eckenhoff, W. T.; Zhu, Y.; Pintauer, T.; Jin, R. *J. Am. Chem. Soc.* **2010**, *132*, 8280-8281.

[65] Knoppe, S.; Dharmaratne, A. C.; Schreiner, E.; Dass, A.; Bu□rgi, T. *J. Am. Chem. Soc.* **2010**, *132*, 16783-16789.

[66] Nimmala, P. R.; Yoon, B.; Whetten, R. L.; Landman, U.; Dass, A. *J. Phys. Chem. A* **2013**, *117*, 504-517.

[67] Levi-Kalisman, Y.; Jadzinsky, P. D.; Kalisman, N.; Tsunoyama, H.; Tsukuda, T.; Bushnell, D. A.; Kornberg, R. D. *J. Am. Chem. Soc.* **2011**, *133*, 2976-2982.

[68] Dass, A.; Nimmala, P. R.; Jupally, V. R.; Kothalawala, N. *Nanoscale* **2013**, *5*, 12082-12085.

[69] Qian, H.; Jin, R. *Chem. Mater.* **2011**, *23*, 2209-2217.

[70] Negishi, Y.; Sakamoto, C.; Ohyama, T.; Tsukuda, T. *J. Phys. Chem. Lett.* **2012**, 1624-1628.

[71] Chaki, N. K.; Tsunoyama, H.; Negishi, Y.; Sakurai, H.; Tsukuda, T. *J. Phys. Chem. C* **2007**, *111*, 4885-4888.

[72] Negishi, Y.; Kurashige, W.; Kobayashi, Y.; Yamazoe, S.; Kojima, N.; Seto, M.; Tsukuda, T. *J. Phys. Chem. Lett.* **2013**, 3579-3583.

[73] Negishi, Y.; Kurashige, W.; Niihori, Y.; Iwasa, T.; Nobusada, K. *Phys. Chem. Chem. Phys.* **2010**, *12*, 6219-6225.

[74] Negishi, Y.; Munakata, K.; Ohgake, W.; Nobusada, K. *J. Phys. Chem. Lett.* **2012**, *3*, 2209-2214.

[75] Niihori, Y.; Kurashige, W.; Matsuzaki, M.; Negishi, Y. *Nanoscale* **2013**, *5*, 508-512.

[76] Kurashige, W.; Munakata, K.; Nobusada, K.; Negishi, Y. *Chem. Commun.* **2013**, *49*, 5447-5449.

[77] Kurashige, W.; Negishi, Y. *J. Clust. Sci.* **2012**, *23*, 365-374.

[78] Negishi, Y.; Igarashi, K.; Munakata, K.; Ohgake, W.; Nobusada, K. *Chem. Commun.* **2012**, *48*, 660-662.

[79] Kumara, C.; Dass, A. *Nanoscale* **2011**, *3*, 3064-3067.

[80] Kothalawala, N.; Kumara, C.; Ferrando, R.; Dass, A. *Chem. Commun.* **2013**, *49*, 10850-10852.

[81] Qian, H.; Barry, E.; Zhu, Y.; Jin, R. *Acta Phys. Chim. Sin.* **2011**, *27*, 513-519.

[82] Kauffman, D. R.; Alfonso, D.; Matranga, C.; Qian, H.; Jin, R. *J. Phys. Chem. C* **2013**, *117*, 7914-7923.

[83] Christensen, S. L.; MacDonald, M. A.; Chatt, A.; Zhang, P.; Qian, H.; Jin, R. *J. Phys. Chem. C* **2012**, *116*, 26932-26937.

[84] Bruma, A.; Negreiros, F. R.; Xie, S.; Tsukuda, T.; Johnston, R. L.; Fortunelli, A.; Li, Z. Y. *Nanoscale* **2013**, *5*, 9620-9625.

[85] Tlahuice-Flores, A. *J. Nanopart. Res.* **2013**, *15*, 1-7.

[86] Fernández, E. J.; Laguna, A.; López-de-Luzuriaga, J. M.; Monge, M.; Olmos, M. E.; Puelles, R. C. *J. Phys. Chem. B* **2005**, *109*, 20652-20656.

[87] Lide, D. R., *CRC Handbook of Chemistry and Physics*. 92th edition, CRC Press: Boca Raton: 2011.

[88] Gómez-Graña, S.; Goris, B.; Altantzis, T.; Fernández-López, C.; Carbó-Argibay, E.; Guerrero-Martínez, A.; Almora-Barrios, N.; López, N.; Pastoriza-Santos, I.; Pérez-Juste, J.; Bals, S.; Van Tendeloo, G.; Liz-Marzán, L. M. *J. Phys. Chem. Lett.* **2013**, *4*, 2209-2216.

[89] Dou, X.; Yuan, X.; Yao, Q.; Luo, Z.; Zheng, K.; Xie, J. *Chem. Commun.* **2014**, *50*, 7459-7462.

[90] Lopez-Acevedo, O.; Akola, J.; Whetten, R. L.; Gro□nbeck, H.; Hakkinen, H. *J. Phys. Chem. C* **2009**, *113*, 5035-5038.

[91] Malola, S.; Hakkinen, H. *J. Phys. Chem. Lett.* **2011**, *2*, 2316-2321.

[92] Ackerman, M.; Stafford, F. E.; Drowart, J. *J. Chem. Phys.* **1960**, *33*, 1784-1789.

[93] Jiang, D.-e.; Dai, S. *Inorg. Chem.* **2009**, *48*, 2720-2722.

[94] Yang, H.; Wang, Y.; Lei, J.; Shi, L.; Wu, X.; Mäkinen, V.; Lin, S.; Tang, Z.; He, J.; Häkkinen, H.; Zheng, L.; Zheng, N. *J. Am. Chem. Soc.* **2013**, *135*, 9568-9571.

[95] Singh, A. K.; Xu, Q. *ChemCatChem* **2013**, *5*, 652-676.

[96] Walter, M.; Moseler, M. *J. Phys. Chem. C* **2009**, *113*, 15834-15837.

[97] Kacprzak, K. A.; Lehtovaara, L.; Akola, J.; Lopez-Acevedo, O.; Hakkinen, H. *Phys. Chem. Chem. Phys.* **2009**, *11*, 7123-7129.

[98] Baksi, A.; Pradeep, T. *Nanoscale* **2013**, *5*, 12245-12254.

[99] Craighead, K. L.; Felicissimo, A. M. P.; Krogstad, D. A.; Nelson, L. T. J.; Pignolet, L. H. *Inorg. Chim. Acta.* **1993**, *212*, 31-39.

[100] Lu, X.; Chen, J.; Skrabalak, S. E.; Xia, Y. *Proc. Inst. Mech. Eng. N J. Nanoeng. Nanosyst.* **2007**, *221*, 1-16.

[101] Wang, C.; Xu, L.; Xu, X.; Cheng, H.; Sun, H.; Lin, Q.; Zhang, C. *J. Colloid Interface Sci. 416*, 274-279.

[102] Murugadoss, A.; Kai, N.; Sakurai, H. *Nanoscale* **2012**, *4*, 1280-1282.

[103] Wu, Z.; Wang, M.; Yang, J.; Zheng, X.; Cai, W.; Meng, G.; Qian, H.; Wang, H.; Jin, R. *Small* **2012**, *8*, 2028-2035.

[104] Zhang, H.; Toshima, N. *Appl. Catal. A-Gen.* **2012**, *447–448*, 81-88.

[105] Kaizuka, K.; Miyamura, H.; Kobayashi, S. *J. Am. Chem. Soc.* **2010**, *132*, 15096-15098.

[106] Sankar, M.; Dimitratos, N.; Miedziak, P. J.; Wells, P. P.; Kiely, C. J.; Hutchings, G. J. *Chem. Soc. Rev.* **2012**, *41*, 8099-8139.

[107] Zhu, Y.; Qian, H.; Drake, B. A.; Jin, R. *Angew. Chem. Int. Ed.* **2010**, *49*, 1295-1298.

[108] Nie, X.; Qian, H.; Ge, Q.; Xu, H.; Jin, R. *ACS Nano* **2012**, *6*, 6014-6022.

[109] Liu, Y.; Tsunoyama, H.; Akita, T.; Tsukuda, T. *J. Phys. Chem. C* **2009**, *113*, 13457-13461.

[110] Liu, H.; Zhang, X.; Wu, X.; Jiang, L.; Burda, C.; Zhu, J.-J. *Chem. Commun.* **2011**, *47*, 4237-4239.

[111] Wang, S.; Meng, X.; Das, A.; Li, T.; Song, Y.; Cao, T.; Zhu, X.; Zhu, M.; Jin, R., *Angew. Chem., Int. Ed.* **2014,** *53*, 2376-2380.

[112] Corma, A.; Garcia, H. *Chem. Soc. Rev.* **2008**, *37*, 2096-2126.

[113] Wilson, R. *Chem. Soc. Rev.* **2008**, *37*, 2028-2045.

[114] Sperling, R. A.; Rivera Gil, P.; Zhang, F.; Zanella, M.; Parak, W. J. *Chem. Soc. Rev.* **2008**, *37*, 1896-1908.

[115] Zhang, Q. B.; Xie, J. P.; Yu, Y.; Lee, J. Y. *Nanoscale* **2010**, *2*, 1962-1975.

[116] Ghosh, A.; Basak, S.; Wunsch, B. H.; Kumar, R.; Stellacci, F. *Angew. Chem. Int. Ed.* **2011**, *50*, 7900-7905.

[117] Liu, X.; Yu, M.; Kim, H.; Mameli, M.; Stellacci, F. *Nat. Commun.* **2012**, *3*, 1182.

[118] Xu, Q.; Kang, X.; Bogomolni, R. A.; Chen, S. *Langmuir* **2010**, *26*, 14923-14928.

[119] Yu, M.; Zhou, C.; Liu, J.; Hankins, J. D.; Zheng, J. *J. Am. Chem. Soc.* **2011**, *133*, 11014-11017.

[120] Niihori, Y.; Matsuzaki, M.; Pradeep, T.; Negishi, Y. *J. Am. Chem. Soc.* **2013**, *135*, 4946-4949.

[121] Tang, Z.; Robinson, D. A.; Bokossa, N.; Xu, B.; Wang, S.; Wang, G. *J. Am. Chem. Soc.* **2011**, *133*, 16037-16044.

[122] Kacprzak, K. A.; Lopez-Acevedo, O.; Hakkinen, H.; Gronbeck, H. *J. Phys. Chem. C* **2010**, *114*, 13571-13576.

[123] Zhou, C.; Hao, G.; Thomas, P.; Liu, J.; Yu, M.; Sun, S.; Öz, O. K.; Sun, X.; Zheng, J. *Angew. Chem. Int. Ed.* **2012**, *51*, 10118-10122.

[124] Kwak, K.; Lee, D. *J. Phys. Chem. Lett.* **2012**, 2476-2481.

[125] Yuan, X.; Zhang, B.; Luo, Z.; Yao, Q.; Leong, D. T.; Yan, N.; Xie, J. *Angew. Chem. Int. Ed.* **2014**, *53*, 4623-4627.

[126] Yee, C. K.; Ulman, A.; Ruiz, J. D.; Parikh, A.; White, H.; Rafailovich, M., *Langmuir* **2003,** *19*, 9450-9458.

[127] Desireddy, A.; Conn, B. E.; Guo, J.; Yoon, B.; Barnett, R. N.; Monahan, B. M.; Kirschbaum, K.; Griffith, W. P.; Whetten, R. L.; Landman, U.; Bigioni, T. P. *Nature* **2013**, *501*, 399-402.

[128] Bakr, O. M.; Amendola, V.; Aikens, C. M.; Wenseleers, W.; Li, R.; Dal Negro, L.; Schatz, G. C.; Stellacci, F. *Angew. Chem. Int. Ed.* **2009**, *48*, 5921-5926.

[129] Laaksonen, T.; Ruiz, V.; Liljeroth, P.; Quinn, B. M. *Chem. Soc. Rev.* **2008**, *37*, 1836-1846.

[130] Xie, J. P.; Zheng, Y. G.; Ying, J. Y. *J. Am. Chem. Soc.* **2009**, *131*, 888-889.

[131] Tang, Z.; Ahuja, T.; Wang, S.; Wang, G. *Nanoscale* **2012**, *4*, 4119-4124.

[132] Gao, C.; Vuong, J.; Zhang, Q.; Liu, Y.; Yin, Y. *Nanoscale* **2012**, *4*, 2875-2878.

[133] Jin, Z.; Xiao, M.; Bao, Z.; Wang, P.; Wang, J. *Angew. Chem. Int. Ed.* **2012**, *51*, 6406-6410.

[134] Guo, W.; Yuan, J.; Wang, E. *Chem. Commun.* **2009**, 3395-3397.

[135] Yu, J.; Patel, S. A.; Dickson, R. M. *Angew. Chem. Int. Ed.* **2007**, *46*, 2028-2030.

[136] Song, Y.; Liu, K.; Chen, S. *Langmuir* **2012**, *28*, 17143-17152.

[137] Guo, X.; Zhang, Q.; Sun, Y.; Zhao, Q.; Yang, J. *ACS Nano* **2012**, *6*, 1165-1175.

[138] Shichibu, Y.; Negishi, Y.; Tsunoyama, H.; Kanehara, M.; Teranishi, T.; Tsukuda, T. *Small* **2007**, *3*, 835-839.

[139] Dass, A. *J. Am. Chem. Soc.* **2009**, *131*, 11666-11667.

[140] Yuan, X.; Tay, Y.; Dou, X.; Luo, Z.; Leong, D. T.; Xie, J. *Anal. Chem.* **2012**, *85*, 1913-1919.

LIST OF PUBLICATIONS

1. **Dou, X.**; Yuan, X.; Yu, Y.; Luo, Z.; Yao, Q.; Leong, D. T.; Xie, J. Lighting Up Thiolated Au@Ag Nanoclusters via Aggregation-Induced Emission. *Nanoscale* **2014**, *6*, 157-161.

2. **Dou, X.**; Yuan, X.; Yao, Q.; Luo, Z.; Zheng, K.; Xie, J. Facile Synthesis of Water-Soluble Bimetallic $Au_{25-x}Ag_x$ Nanoclusters Protected by Mono- and Bi-thiolates. *Chem. Commun.* **2014**, *50*, 7459-7462.

3. Yuan, X.; **Dou, X.**; Zheng, K.; Xie, J. Recent Advances in the Synthesis and Applications of Ultrasmall Bimetallic Nanoclusters. *Part. Part. Syst. Char.* **2014**, to be submitted. (Review article)

4. Yuan, X.; Tay, Y.; **Dou, X.**; Luo, Z.; Leong, D. T.; Xie, J. Glutathione-Protected Silver Nanoclusters as Cysteine-Selective Fluorometric and Colorimetric Probe. *Anal. Chem.* **2013**, *85*, 1913-1919.

5. Yuan, X.; Yao, Q.; Yu, Y.; Luo, Z.; **Dou, X.**; Xie, J. Traveling through the Desalting Column Spontaneously Transforms Thiolated Ag Nanoclusters from Nonluminescent to Highly Luminescent. *J. Phys. Chem. Lett.* **2013**, *4*, 1811-1815.